공학박사학위논문

Engineering and Validation of Open Microfluidic Platform for Organ on a Chip

인공생체 칩을 위한 개방형 미세유체 플랫폼의 공학적 설계 및 검증

2018 년 2 월

서울대학교 대학원

기계항공공학부

탁 동 하

Engineering and Validation of Open Microfluidic Platform for Organ on a Chip

인공생체 칩을 위한 개방형 미세유체 플랫폼의 공학적 설계 및 검증

지도교수 전 누 리

이 논문을 공학박사 학위논문으로 제출함

2017 년 11 월

서울대학교 대학원

기계항공공학부

탁 동 하

탁동하의 공학박사 학위논문을 인준함

2017 년 12 월

위 원 장 : 최 만 수

부위원장 : 전 누 리

위 원 : 고 승 환

위 원 : 김 태 일

위 원 : 윤 호 영

Abstract

Engineering and Validation of Open Microfluidic Platform for Organ on a Chip

Dongha Tahk

Department of Mechanical and Aerospace Engineering

College of Engineering

Seoul National University

Open microfluidic device was developed using the open-access microfluidic device with through-hole membrane for the regenerative medicine of Peripheral arterial disease (PAD). PAD is commonly defined as narrowing of blood vessels in the lower part of arteries or arterioles. Major risk factors of occurrence of PAD include smoking, hypertension, hypercholesterolemia, atherosclerosis, and complications of diabetes. To develop safe and effective procedures for vascularized tissue injection, we focused on open microfluidic device using through-hole membrane and open-access microfluidic device system. For the transplantable tissue

culture, simple fabrication method of through-hole membrane was developed for the media supply to the tissue. Due to the small scale of the fabricated pores, the construction of through-hole membranes on a large scale and with relatively large areas faces many difficulties. Novel fabrication methods for a large-area, freestanding micro/nano through-hole membrane constructed from versatile membrane materials using through-hole membranes on a microfluidic chip (THMMC) for the reconstitution of 3D tissue. The through-hole site was easily customizable from the micro to the nanoscale, with a low or high aspect ratio giving rise to reliable membranes. Also, the rigidity and biocompatibility of the through-hole membrane are easily tunable by simple injection of versatile membrane materials to obtain a large area (up to 3600 mm^2). And we describe a simple, versatile method of generating open-access microfluidic device (OAMD) with possible non-destructive tissue sampling for TEM imaging. Generally, the analysis of organ-on-a-chip usually applied by optical microscope, fluorescence microscope and confocal microscopy. Although optical imaging technologies are widespread and effective observational tools, they possess functional and resolution limitations. The myelination by Schwann cells is critically important in restoring neuromuscular motor function after injury or

peripheral neuropathy, and in the case of quantifying myelination, transmission electron microscope (TEM) analysis is a requisite. The proposed OAMD platform incorporated a novel biocompatible self-detachable photopolymer (BSP) substrate to provide a viable closed microphysiological system culture environment while also allowing for controllable and nondestructive tissue sampling for TEM analysis. Furthermore, We herein thesis a novel transplantable tissue engineering technique that yields functional and vascularized tissue that can be successfully transplanted into the Balb C Nu nude mouse using THMMC and OAMD technology.

Keywords: Microfluidic, Organ on a Chip, Regenerative Medicine, Tissue Engineering, Transplantation

Student number: 2010-30797

Contents

List of Figures

Chapter 1

Introduction

1-1. Open Microfluidic Platform

Microfluidics [1] as a field has rapidly developed over the last few decades as a means of replicating human in vivo [2] rheological conditions and conducting single cell scale analysis [3] for drug screening and drug delivery system development. [4] Human biomimetic microfluidic devices are often referred to as 'organ on a chip' [5, 6] systems, and span various organs and tissues, such as lungs, [7] guts, [8] skin, and kidneys. [9] These chips rely on through-hole membranes to emulate human in vivo rheological conditions for cell-to-cell and tissue-to-tissue separation layers. Additionally, microfluidic devices [10] have also been applied to single cell trapping techniques. [11] Although organ on a chip has high precision mimic system, it suffers from the disadvantages inherent in the collection for analysis and transplantation of cells in a closed system, as cells are not accessible for re-collection once they have been analyzed.[12] In this thesis proposed the engineering and validation of open microfluidic

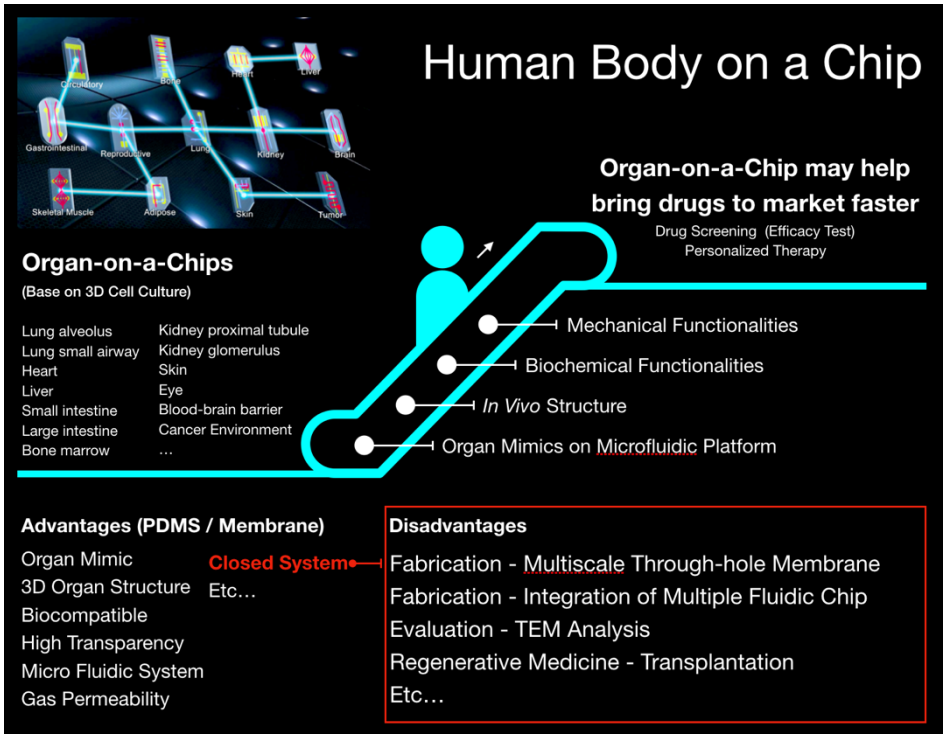

Figure 1-1. The system of human body on a chip for high throughput of drug screening. The organ on a chip has developed as diverse advantages by PDMS closed system. However, the closed system has disadvantages for the nondestructive tissue sampling and transplantation.

platform for the advanced organ on a chip analysis and application of the tissue engineering. The organ on a chip was well designed system for the three-dimensional tissue culture system by PDMS closed system. However, by the closed system, it has the disadvantage of nondestructive tissue sampling and transplantation. For the open microfluidic device, the through-hole membrane which was commonly used as a part of the organ on a chip, and self-detachable film which was used for the nondestructive tissue sampling was needed.

1-2. Novel Fabrication Process of Through-hole Membrane

An alternate method utilizing a micro/nano membrane made of biocompatible PDMS [13] for cell trapping allows for the collection of cells after they have already been analyzed - though, this method requires a membrane that is comparatively more difficult and less efficient to fabricate.[14] Conventionally, the through-hole membrane is fabricated by MEMS processes such as imprinting [15] or micromolding in capillaries (MIMIC). [16, 17, 18, 19] The imprinting process involves applying a liquid pre-polymer to a flat surface, and then pressing a positive

pillar patterned mold into the pre-polymer layer. Imprinting exhibits disadvantages concerning residues around the cast perforations due to the inherent nature of the viscosity and wetting characteristics of the membrane pre-polymer. Should the pressure applied to the positive pillar patterned mold prove insufficient, the imprinting process may leave an undesirable closed negative structure within the membrane rather than a complete hole. As such, the applied pressure on the pillar patterned mold must be tuned depending on the viscosity of the membrane pre-polymer. Due to the critical nature of accounting for applied pressure and membrane pre-polymer viscosities, the reliable fabrication of uniformly thick and reliably patterned large area membranes is quite difficult. Other conventional fabrication methods such as MIMIC, manual punching, spin coating, and MEMS-based etching also harbor unsuitable characteristics. For instance, MIMIC, which involves capillary driven injection, is not suited for large area membrane fabrication. Manual punching using a gauged needle or biopsy punch is both time consuming and limited in size due to the availability of the punch. Spin coating results in the formation of a defective meniscus at the perforation site, and may even result in an unwanted residual layer if the spin conditions are not precisely controlled. Conventional MEMS-based etching [20] requires expensive machinery

for fabrication, and also involves toxic gases in the fabrication process. In a novel fabrication procedure proposed by Cho et al., [21] micro and nano scale through-holes can be produced comparatively more conveniently and accurately through the use of a hierarchical mold under specially confined pressure conditions.

This thesis describes a novel fabrication method for a multiscale through-hole membrane on a microfluidic chip (THMMC). Membrane fabrication takes place in three steps beginning with plasma bonding of the top part of a PDMS microfluidic chip with a flat or nano-patterned substrate. Secondly, the membrane material (pre-polymer) is injected through a microfluidic channel then cured. Lastly, the mem- brane is separated from the microfluidic chip via cutting and mechanical force. This novel fabrication process does not apply any pressure to the top and bottom components, especially during curing of the pre-polymer. The diameter of the fabricated through-hole membrane created through this process ranges from a hundred micrometers to a hundred nanometers, depending on the positive patterned top and bottom components. The nano through-hole membrane is fabricated as a hierarchical structure. The microfluidic channel, as the top part component, supports the handle area for the micro- pillar plasma-bonded with the nanopillar patterned

substrate which was the section of the nano through-hole membrane area. The hierarchically structured nano through-hole mem- brane exhibits high durability and stability, with significant resistance to tearing when the through-hole site has a low aspect ratio (<1) and sub-micrometer thickness near the opening. This novel fabrication method gives a high yield and is viable for large area (3600 mm^2) production using a 4 inch wafer-based microfluidic chip mold. The through-hole membrane was obtained from a freestanding [22] film and the shape can be tuned as pillar and conical [23, 24] types. The membrane rigidity can be altered by the pre-polymer injection method.

1-3. Open-Access Microfluidic Device for TEM Analysis

Given the controversy surrounding the ethics of animal testing, recent trends have seen an increase of animal testing bans on ethical grounds. [25] To address the demands of *in vivo* testing results without the use of animal, organ on a chip technologies were developed to deliver *in vivo* like *in vitro* tissue culture platforms. Organ on a chip platforms are generally comprised of microstructured biocompatible devices, such as PDMS, plasma bonded to glass. To mimic *in vivo* structures, biomimetic

platforms have largely adopted three-dimensional cell culture techniques such as micropost compartmentalized microfluidic coculture devices. [26, 27] These biomimetic platforms, like lung on a chip, liver on a chip, and lung on a chip, were designed to mimic specific human organ functions as closed microphysiological systems. [28, 29, 30, 31] However, microfluidic devices operate as closed systems, wherein coculture and microchannel chambers are confined between permanently bonded PDMS and glass. Generally, the analysis of organ on a chip usually applied by optical microscope and confocal microscopy. Although optical imaging technologies are widespread and effective observational tools, they possess functional and resolution limitations. [32] Observation of phenomena like the axonal myelination of motor neurons by Schwann cells require nanometer scale resolution that is infeasible using conventional optical imaging. [33, 34, 35] In the case of quantifying myelination, confirming histological responses to drug administration, and other subtle and difficult to image phenomena, transmission electron microscope (TEM) analysis is a requisite. As conventional closed microfluidic devices prevent the nondestructive retrieval of tissues for analysis, there is a need for an openly accessible alternative which permits for higher resolution imaging. An open microfluidic chip could also see

potential use in application like chemotactic *in situ* mRNA isolation, and open channel studies. [36, 37, 38, 39]

1-4. Transplantation of 3D Tissue as Regenerative Medicine

Peripheral arterial disease (PAD) is commonly defined as narrowing of blood vessels in the lower part of arteries or arterioles. Major risk factors of occurrence of PAD include smoking, hypertension, hypercholesterolemia, atherosclerosis, and complications of diabetes [40]. According to a survey, PAD is prevalent and more than 5 million adults suffered from PAD in the United States [41]. In the PAD progression, patients might have limb pain with ischemic ulceration and gangrene. In the late stages of PAD, major limb amputation may be required [42]. Cellular implantation, a technique involving the injection of tissue into the PAD, was developed as an alternative therapeutic strategy for PAD failure. Several studies of PAD using various cell sources have successfully demonstrated improved function of the damaged vessel and subsequent regeneration of new vessels. However, significant problems are associated with cellular PAD due to the low nutritional supply in the tissue, and a proper anchoring matrix. Hence, the creation of an acceptable cell environment is a central issue in the need to improve the effectiveness of

regenerative medicine. To address the limitations of cellular PAD, a tissue engineering approach was developed to provide alternatives. The organ changes its shape from a sheet-like arrangement with primitive cells to mature three-dimensional structures through morphogenetic processes. [43, 44, 45] As regenerative medicine, a wide range of biomaterials have been used for the total or partial replacement of damaged organs and/or tissue structures. [46, 47, 48] As the functions of the living organ are realized by periodic changes in the lateral arrangement of tissue elements, multiform scaffold systems mimicking the native tissue are desired. The casting and electrospinning have been introduced to fabricate diverse scaffolds. [49, 50] However, these fabrication processes have limitations for organ like structure productions. Although recent progress in tissue engineering has focused on using 3D printer schemes, there are still limitations such as the shortage of appropriate printing materials and technical challenges related to the sensitivity of living cells. [51, 52, 53, 54]

Chapter 2

Rapid large area fabrication of multiscale through-hole membranes

---

2-1. Introduction

There are many proposed mechanisms by which single cells can be trapped; among them is the through- hole membrane for the characterization of individual microorganisms. Due to the small scale of the fabricated pores, the construction of through-hole membranes on a large scale and with relatively large areas faces many difficulties. This thesis describes novel fabrication methods for a large-area, freestanding micro/nano through-hole membrane constructed from versatile membrane materials using through-hole membranes on a microfluidic chip (THMMC). This process can rapidly (<20 min) fabricate membranes with high fidelity multiscale hole size without residual layers. The through-hole site was easily customizable from the micro to the nanoscale, with a low or high aspect ratio giving rise to reliable membranes. Also, the rigidity and biocompatibility of the through-hole membrane are easily

tunable by simple injection of versatile membrane materials to obtain a large area (up to 3600 mm^2).

2-2. Materials and Method

2-2-1. Through-Hole Membrane by Microfluidic Chip (THMMC)

The experimental through-hole membrane was fabricated by applying pre-polymer membrane material through a PDMS microfluidic chip patterned with distribution channels into a mold. For microscale membrane production, the PDMS microfluidic prepolymer distribution chip is also patterned with positive micropillars and plasma bonded to a flat surface backer, like glass in Figure 2-1. With nanoscale membranes, the membrane molding chamber of the PDMS chip is bonded to a nanopatterned PEG-DA surface rather than a flat glass backer in Figure 2-3. The bottom of the entire membrane is embedded with nanopatterning, with the actual transmembrane pores existing where the nanopatterned posts of the PEG-DA backer overlap with the PDMS microposts. Post injection, the assemblies are cured and then the membranes are mechanically extracted for use. The negative micropillar patterned master

was fabricated using a conventional lithography process with SU-8 photoresist [55] (SU-8 100, MicroChem. the USA) for the positive micropillar patterned microfluidic chip. The mold was replicated from the negative patterned SU-8 master using PDMS (Sylgard 184, Dow Corning, USA). The comparatively large inlet/outlet ports were punched via 1mm medical grade skin biopsy punch (diameter 1 mm, Picu Punch) for membrane material injection channels. The PEG-DA surfaces were fabricated using the UV replica molding method in which PEG-DA UV curable solution was mixed with 97% (by mass) of polyethylene glycol diacrylate (PEG-DA, Mn 250, Sigma-Aldrich, viscosity 15 ~ 35 cP) pre-polymer with 3% (by mass) of 1-hydroxy-cyclohexyl-phenyl-ketone (Irgarcure 184, BASF) as photo-initiator. The UV curable PEG-DA solution was applied to a Si wafer for fabrication of the flat substrate, and on a nano/micro patterned silicon master for the fabrication of the positive nano/micro patterned substrate. A flexible and clear polyester film was pretreated on both sides for enhanced adhesion to the UV curing resin (Thickness: 100 μm, skyrol V7200, SKC, Korea), was then placed on the UV resin and roll-pressed against the liquid ten times at a pressure of 2 ~ 3 bars. The PEG-DA layer thickness was measured to be 30 ~ 40 μm after pressure rolling. [13] Next, the PEG-DA layer was cured under UV light

for 120 seconds (UV wavelength: 250–400 nm, dose: 100 mJ/cm^2). After separating the PE backing panel from the wafer, a flat PEG-DA sheet was obtained on the PE Film. The PEG-DA replica mold was duplicated from a negatively patterned silicon master mold using the same protocol as the flat PEG-DA mold.

2-2-2. Distribute Microfluidic Channel

A PDMS based microfluidic distribution chip was designed with a network of microfluidic channels to facilitate the efficient and bubble-less application of membrane pre-polymer across a 60 mm x 60 mm wide area during the material injection process in Figure 2-1.

2-2-3. Micro / Nano Membrane

The membrane was fabricated in three simple steps in Figure 2-1b. The first step combines plasma bonding of the top part of a PDMS microfluidic chip with a flat or nanopatterned substrate. The microfluidic chip for a through-hole membrane was created using air plasma at the fixed condition of 45 sccm, 50 mTorr, 50 W, and 1 min (CUTE MPR, Femto Science, Korea), leaving behind a microfluidic channel with a flat surface

for the microscale membrane. For the nanoscale through-hole membrane, the PDMS microfluidic channel was created using air plasma bonding with a nanopillar patterned substrate at the same fixed condition, which was made by the PEG-DA nano patterned mold. The second step is injection and curing, in which the membrane material (pre-polymer) is injected through the microfluidic distribution channels then cured. The inner surfaces of the PDMS microfluidic chip were coated with a fluoropolymer to decrease inner surface energy, carried in a solution of 2 % (by mass) of Polytetrafluoroethylene (PTFE, Teflon, Dupont) in 98% (by mass) of solvent (Fluorinert FC-40, 3M). [56] The PDMS pre-polymer mixture with the curing agent was then injected into the microfluidic channel using a syringe pump at a flowrate of 0.1 ml/min. The PDMS membrane was then cured for 2 h at 70 °C. As the PDMS membrane was plasma bonded to a slab of PDMS for easy separation from the microfluidic chip, the membrane exhibits high flexibility and low mechanical modulus. There was a variety of UV curable materials injected into the microfluidic chip utilizing a syringe pump (0.1 ml / min) without any additional fluorinated coating processes about the intra surface of PDMS microfluidic chip. When curing the membrane materials, the chip was exposed to UV light for 180 s (UV wavelength = 250–400 nm, dose

= 100 mJ/cm^2). The third, step is separating the membrane by mechanical failure, using a scalpel and a mechanical force. The PDMS microfluidic chip edge was severed using a scalpel and the micro/nanopillar substrate was separated using cohesive mechanical failure on the bottom surface after curing.

2-3. Results and Discussion

2-3-1. Microscale Through-hole Membrane

Microfluidic pre-polymer distribution chips were fabricated through conventional means with single injection ports to the sides, each branching into four distribution channels for even pre-polymer application. Micro scale membranes were fabricated using a flat glass or flat PEG-DA coated PE film as backers in Figures 2-1. PDMS/Glass plasma bonding is a well-known combination for microfluidic research but PDMS/PEG-DA is relatively uncommon. PDMS/PEG-DA plasma bonding was processed under the same plasma treatment conditions as PDMS/Glass plasma bonding, but post thermal treatment was applied at 150 ℃ for 5 min in order to mitigate injection pressure induced material failure. Figure 2-3

shows a 3600 mm^2 PDMS micro-through-hole array membrane with 80 μm diameter holes and 200 μm spacing between holes. As shown in Figures 2-2a-i-iv, through-hole fabrication succeeded in generating high-accuracy holes throughout the membrane, with an aspect ratio of 0.8, and no detectable meniscus formation at the edge of each hole site. As demonstrated, it is possible to generate high accuracy through hole arrays on a large area membrane. Membranes produced in this manner can be easily integrated to other PDMS based microfluidic chips via plasma bonding in a modular manner for a myriad of diagnostic designs. Thin PDMS membranes with microscale thickness also have many applications in flexible display and electronically sensitive surface technologies due to high flexibility and conformal contact adhesion characteristics. Figures 2-2 show the versatility of producible through-hole shapes, sizes, and aspect ratios using modifiable casting components to vary output to the desired specification. The device cast in Figure 2-2c was fabricated using a smaller micropattern than that of Figure 1c, and was observed to have a higher aspect ratio of 2.5. Controlled over-exposure to UV in the SU-8 photoresist master can be used to generate conical through-holes. With all other fabrication protocols held constant, the demonstration model conical membrane was shown to have top through-hole diameters of 25 μm and

bottom diameters of 9 μm. The membrane materials applied was polyurethane acrylate UV curable resin. The through-hole membrane was successfully fabricated for the low and high aspect ratio through-hole membrane or conical type as the diameter of the holes ranged from 80 μm to 9 μm. Following this research, the diverse rheology at the through-hole site which based on the solidified polymeric membrane was easily tunable using diverse micropillar arrayed microfluidic chips.

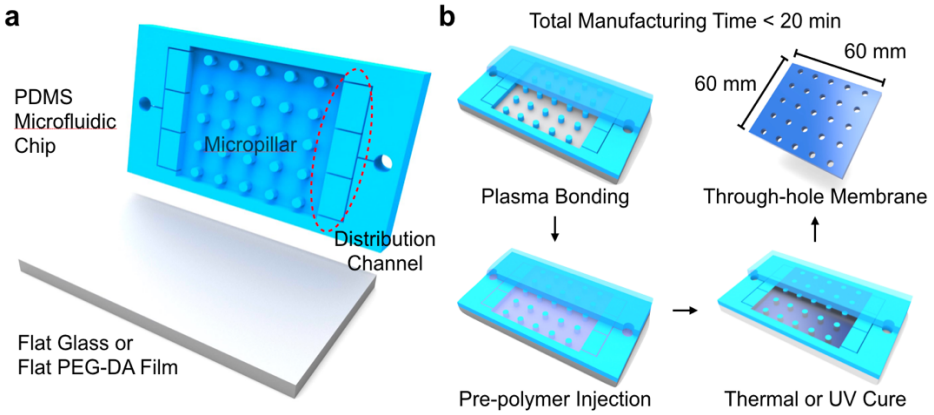

Figure 2-1. a) Components of microscale through-hole membrane fabrication using a microfluidic chip. The top part of the fabrication assembly is a PDMS based microfluidic membrane pre-polymer distribution chip for the controlled and even application of membrane pre-polymer to the micro/nano scale pillar patterning mold below. The substrate used was a flat glass or PEG-DA coated polyethylene film. b) Schematic illustration for fabrication of the microscale through-hole membrane. Protocol consists of plasma bonding, polymer injection & curing and separation steps. The total membrane area was 60 mm by 60 mm using 4-inch base PDMS microfluidic chip.

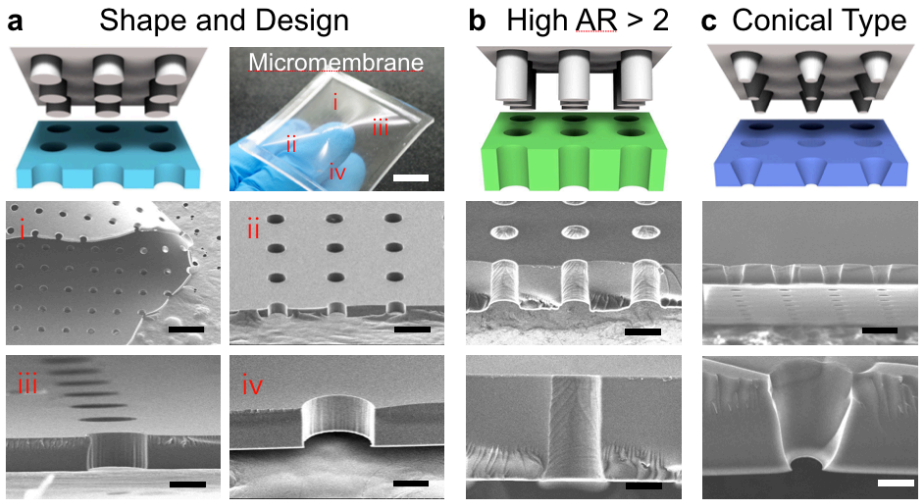

Figure 2-2. a) PDMS through-hole membrane (size: 6 x 6 cm^2) and i~iv) FE-SEM image, respectively. This micromembrane has a low aspect ratio (AR: 0.8). The scale bar indicates a) 1 cm, a-i) 800 μm, a-ii) 200 μm, a-iii) 60 μm, a-iv) 40 μm. b) Illustration images of high aspect ratio (AR: 2.5) micromembrane. Cross-sectional image and magnitude image of high AR micromembrane. Hole diameter was 40 μm. The scale bar indicates 50 μm and 30 μm. c) Illustrations of conical micromembrane and cross sectional image of conical type through-hole membrane. The upper hole diameter was 25 μm and lower hole diameter was 9 μm. The scale bar indicates 50 μm and 10 μm.

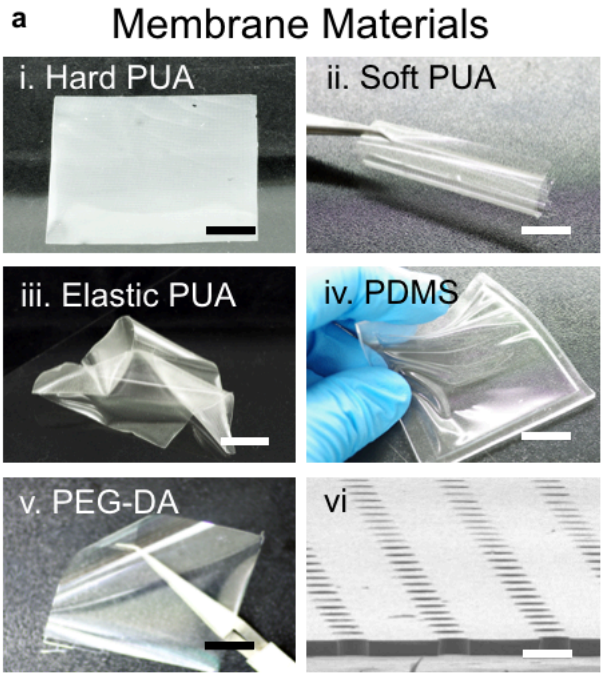

Figure 2-3. a) Variety of membranes made by the following materials; Hard-PUA, Soft-PUA, Elastic-PUA, PDMS and PEG-DA. The hole diameters of (80 μm) and space (200 μm) of f-i~v) were the same structure as a FE-SEM image of f-vi). The scale bar indicates i ~ v) 1cm and vi) 100 μm.

While Figure 2-4 shows only the circular ‘dot’ patterned pores, other shapes like arrow, diamond, square brackets, semicircular arch, star, in any combination, can also be fabricated. The diversity of pore shapes can lead to a highly flexible platform with many applications, such as cell-cell and cell-tissue studies, synthesis, and more.

The micro-membrane is able to be fabricated using a variety of materials, though most of the devices used for cell culturing in this thesis are made of thermo-curable and highly biocompatible PDMS. In addition to thermally curable polymers like PDMS, there are also UV curable materials like PEG-DA (Polyethyleneglycol diacrylate) which were also used. PEG-DA, which is both biocompatible and has a low (20 ~ 30 cP) viscosity while in the liquid prepolymer state, was used to cast the membrane depicted in Figure 1f. Other UV curable polymers were also selected for various mechanical and chemical properties and cast into through hole membranes for testing. Such polymers used, and their corresponding are as follows: hard-PUA (polyurethane acrylate) (E : > 320 MPa, 100 ~ 150 cP) [57], soft-PUA (E : ~ 19.8 MPa, 200 ~ 260 cP), [57] and elastic-PUA (E : ~ 2 MPa, 2500 ~ 2600 cP) [58] at similar level of PDMS (E : ~ 2 MPa, 3500 cP). As all membrane polymers were directly applied to the casting surface through PDMS based microfluidic channels,

all pre-polymer material viscosities needed to be accounted for. PEG-DA, hard-PUA, and soft-PUA, having low viscosity values, were injected at a 1 ml/min rate, while elastic-PUA and PDMS with their high viscosity values were injected at 0.2 ml/min. Accounting for the viscosities of membrane pre-polymers during microchannel injection allowed for the mitigation of unwanted residue formation during the casting process. It is interesting to note, however, that microscale casting can take place without accounting for viscosity under values of up to 3500 cP.

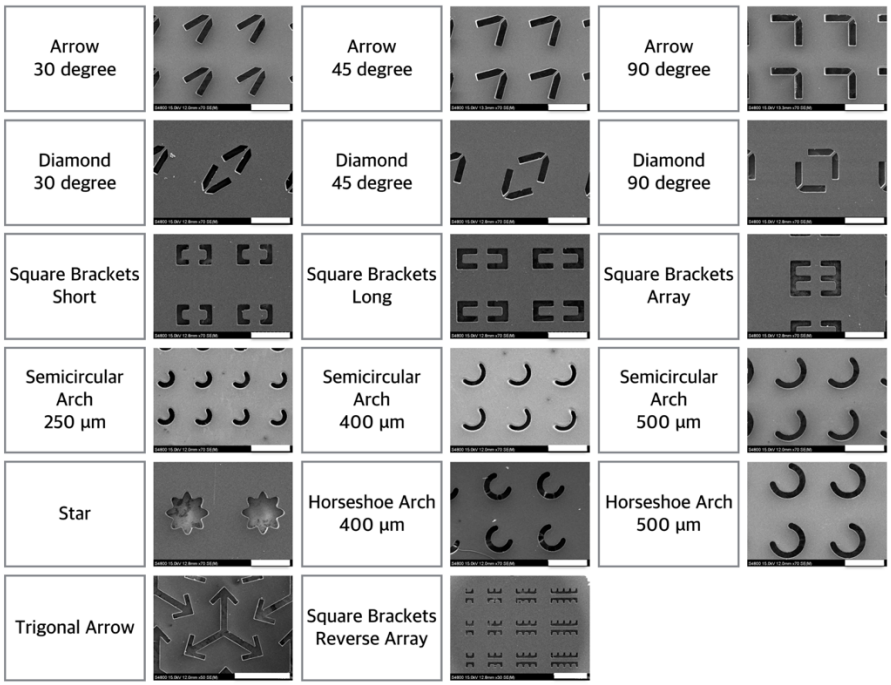

Figure 2-4. A detailed SEM image for the diverse design of micro membrane. All of the white scale bar indicates 500 μm except trigonal arrow and square brackets reverse array (1cm).

2-3-2. Nanoscale Through-hole Membrane

In Figures 2-5 nanoscale through-hole membranes are fabricated through the use of a plasma bonded micropillar arrayed PDMS microfluidic channel with a nanopillar patterned PEG-DA mold. The diameter and height of the nanopillar pattern were 400 nm and 740 nm (an aspect ratio of 1.6), respectively. This interconnection makes a nano through-hole site though a simplified process that does not require a hierarchical mold. Generally, nanoscale membranes of this type suffer from low fracture toughness, especially at thicknesses around or under 100 nm. To help mitigate the thickness induced mechanical frailty, hard-PUA (MINS 311RM) was selected for its high Young's Modulus (>320 MPa) as the membrane material. An 80μm thick hierarchical structure, designed for high fracture resistance, was also implemented to further strengthen the membrane. The microfluidic channel replica was designed as a support frame for the nanomembrane in the entire membrane area. The hexagonal area in Figure 2-6 represents the nano through-hole site, while the planar area represents a support area. As shown in the cross sections in Figures 2-6-ii-iv, the fabricated nano-hole membrane has a thickness of 740 nm and a hole diameter of 400 nm.

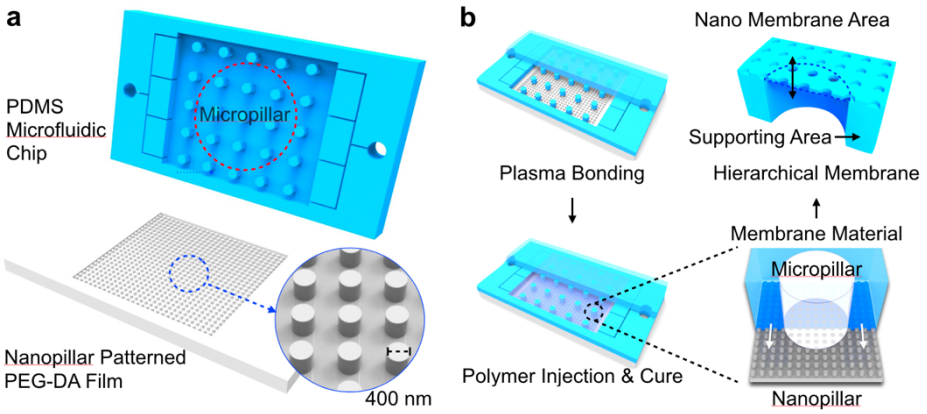

Figure 2-5. a) Illustration of the hierarchical nanoscale through-hole membrane from a microfluidic chip bonded with a nanopatterned substrate. b) Schematic illustration of the fabrication of a nanoscale through-hole membrane. Protocol consisted of plasma bonding, polymer injection & curing and separation steps. The nano through-hole area was fabricated within the plasma bonded area comprising of the micropillar and nanopillar contact area.

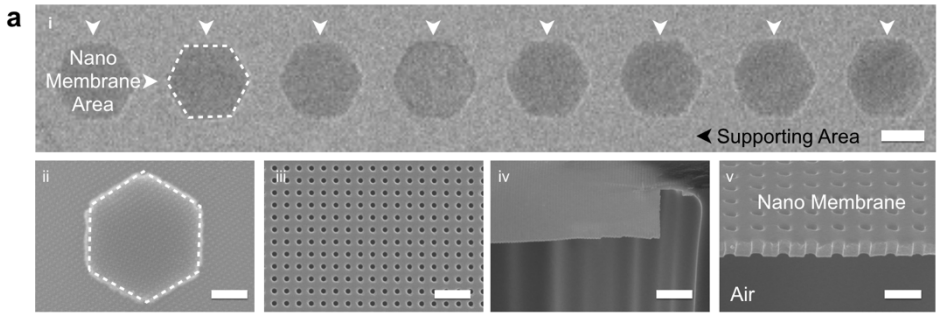

Figure 2-6. a-i) Eight honeycomb structured areas were nanomembrane areas. The other areas were closed areas for membrane support. a-ii, iii) Top view image of one nano through-hole membrane where the moire patterns were obtained at low magnitude scale and magnitude image of nano through-hole area. a-iv, v) Cross-sectional image of nano through-hole membrane. The nanoscale through-hole membrane was obtained. The scale bar indicates i) 300 μm, ii) 100 μm, iii) 2 μm, vi) 10 μm and v) 1 μm.

2-4. Conclusion

This thesis presents a simple approach to the fabrication of micro and nano scale through-hole membranes. Fabrication takes place in a three step process of plasma bonding, membrane material injection and curing, and then the extraction of the completed membrane. The process itself is highly scalable, modular, and compatible with a very diverse range of different polymers to achieve desired specifications. Based on the intra structure rheology of microfluidic chip, the membrane pore diameter was decreased from hundreds of microns to hundreds of nanometers. Through-hole structures can be fabricated in both cylindrical pillar type and conical types, with many options of customizing height, width, and aspect ratio to desired specifications. Using this process, fabricated membranes have a high degree of uniformity of thickness, no residues, and no meniscus deformation at the through-hole sites.

Chapter 3

Open-Access Microfluidic Device for TEM analysis of 3D Reconstituted Myelin Sheaths

3-1. Introduction

Here, we describe a simple, versatile method of generating open-access microfluidic device (OAMD) with possible non-destructive tissue sampling for TEM imaging. Generally, the analysis of organ-on-a-chip usually applied by optical microscope, fluorescence microscope and confocal microscopy. Although optical imaging technologies are widespread and effective observational tools, they possess functional and resolution limitations. The myelination by Schwann cells is critically important in restoring neuromuscular motor function after injury or peripheral neuropathy, and in the case of quantifying myelination, transmission electron microscope (TEM) analysis is a requisite. As conventional closed microfluidic devices prevent the nondestructive retrieval of tissues for analysis, there is a need for an openly accessible alternative which permits for TEM imaging. The proposed OAMD

platform incorporated a novel biocompatible self-detachable photopolymer (BSP) substrate to provide a viable closed microphysiological system culture environment while also allowing for controllable and nondestructive tissue sampling for TEM analysis. BSP is also capable of high fidelity UV lithographic nanoimprinting which can be useful for topography mediated cell behavioral studies. With the added capability of nondestructive tissue sampling, the OAMD platform shows promise as a bridge between the precision and controllability of closed microphysiological culturing and the capability for high resolution imaging and analysis.

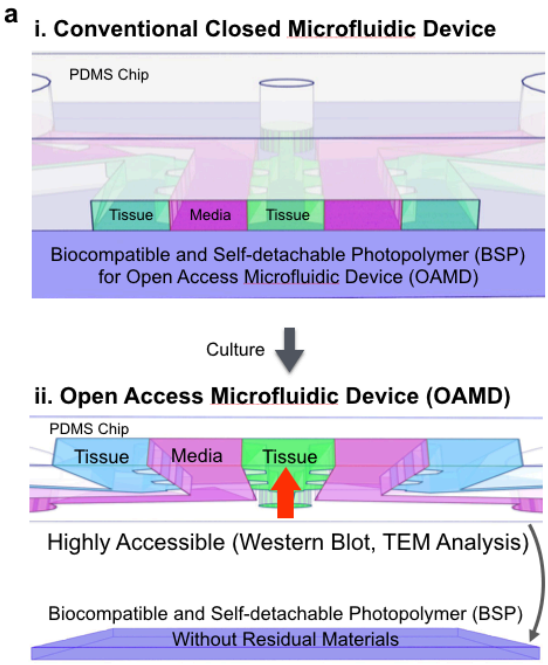

Figure 3-1. a) The open-access microfluidic device (OAMD) was composed of biocompatible and self-detachable photopolymer (BSP) as a substrate material which was plasma-bondable with PDMS microfluidic chip. The initial cell plating condition is equal with conventional PDMS/Glass chip. The BSP film was spontaneously detached from the PDMS chip caused by hydrolysis cleavage of the interface. The Western Blot and TEM analysis of reconstituted tissue was available by external access.

The proposed open-access microfluidic device (OAMD) serves as a non-destructively externally accessible microfluidic coculture platform as shown in Figure 3-1. In this thesis, a conventional PDMS microfluidic three-dimensional cell culture chip was plasma bonded to a BSP instead of glass to provide both closed system culture capabilities as well as nondestructive tissue accessibility. [59] The various BSP formulations were engineered out of biocompatible UV curable materials capable of plasma bonding and separation from PDMS while maintaining tissue integrity for the open-accessibility. BSP formulations were developed with considerations for plasma bondable hydroxyl groups on the surface. Solid BSP surfaces tend to have a high level of flatness, and short crosslinking time, a high degree of bonding strength and a low degree of chemical reactivity to organic solvents. [60] Formulations also require the capacity for UV nanoimprinting lithography (UV-NIL) patterning. In all, the proposed BSP substrate is plasma bonded to PDMS while maintaining both optical transparency and the ability to allow for the nondestructive retrieval of cultured tissues. During the cell culture process, the BSP substrate detaches from PDMS gradually through the absorption of culture medium without tissue damage, and separates from the culture tissue without leaving residues.

Schwann cells form an electrically insulating multilayer sheath of myelin around the axon of motor neurons. This myelin sheath protects neuronal axons, provides nutritional support, and facilitates the conduction of action potential propagation throughout the nervous system. Myelination defects such as delayed myelination, demyelination, or hypomyelination are known cause of serve nervous system disorders. [61, 62, 63, 64] Due to the clinical importance of myelin in nervous system disease models, myelination is a significant area of research. Current *in vitro* models of myelination utilize TEM analysis to observe myelination in petri dish culture tissue. [65, 66, 67, 68, 69, 70, 71] Compared to the conventional petri dish culture *in vitro* platforms, microfluidic cell culture devices have superior tissue level reconstitution control and lower culture media consumption, and are generally superior to conventional petri dish culture methods for 3D cell culturing applications. Furthermore, the OAMD improves on previous microfluidic platforms by adding the possibility if utilizing TEM imaging to confirm pre-myelination and myelination, a feat which was previously highly difficult in PDMS/glass closed microfluidic devices. For this publication, the OAMD platform was utilized to induce myelination on a coculture of motor neurons and Schwann cells, and

verified myelination through TEM imaging of tissues nondestructively sampled directly from the chip.

3-2. Materials and Method

3-2-1. Biocompatible and Self-detachable Photopolymer

As showed in figure 3-2, the main binder was composed three kinds of materials; PEG-DA, TMPTA and HDDA with a photoinitiator. The PEG-DA surfaces were fabricated using the UV replica molding method in which PEG-DA UV curable solution was mixed with 97 wt% (by mass) of Polyethylene glycol diacrylate (PEG-DA, Mn 250, Sigma-Aldrich, viscosity 15 ~ 35 cP) pre-polymer with 3 wt% of 1-hydroxy-cyclohexyl-phenyl-ketone (Irgarcure 184, BASF) as photo-initiator. The BSP-1 is formulated as 29 wt% of Hexan-1,6-dioldiarcrylate (HDDA, M200, Miwon Specialty Chemical, South Korea) with 39 wt% of Trimethylopropane triacrylate (TMPTA, M300, Miwon Specialty Chemical, South Korea) prepolymer with 29 wt% of PEG-DA with 3 wt% of 1-hydroxy-cyclohexyl-phenyl-ketone (Irgarcure 184, BASF). The BSP-2 was mixed with 38 wt% of HDDA, 59 wt% of TMPTA and 3 wt% of PI (Igarcure 184) without the PEG-DA component. A flexible and clear polyester film was pretreated on both sides for enhanced adhesion to the UV curing resin (Thickness: 100 μm, skyrol V7200, SKC, Korea), was then placed on the UV resin and roll-pressed against the liquid ten times at a pressure of 2 ~ 3 bars. The PEG-DA layer thickness was measured to

be 30 ~ 40 μm after pressure rolling. [60] Next, the BSP layer was cured under UV light for 60 seconds (UV wavelength: 250–400 nm, dose: 100 mJ/cm^2). After separating the PE backing panel from the wafer, a flat PEG-DA sheet was obtained on the PE Film. The BSP replica flat film was fully cured during 24 hours at same dose condition for biocompatibility.

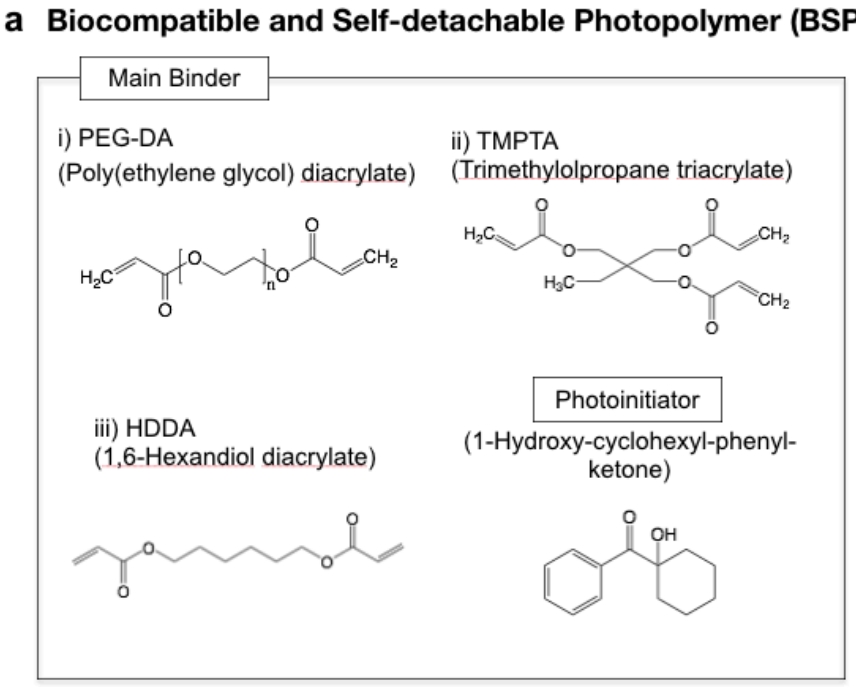

Figure 3-2. a) The biocompatible and Self-Detachable Photopolymer (BSP) was composed as UV-curable pre-polymer. The main binder was composed three kinds of materials; PEG-DA, TMPTA and HDDA with a photoinitiator.

3-2-2. Open-Access Microfluidic Device

The negative micro structured master was fabricated using a conventional lithography process with SU-8 photoresist (SU-8 100, MicroChem. the USA) for the positive micro structure patterned microfluidic chip. The mold was replicated from the negative patterned SU-8 master using PDMS (Sylgard 184, Dow Corning, USA) as 10:1 ratio PDMS and curing agent.[18] The comparatively large inlet/outlet ports were punched via medical grade skin biopsy punch (diameter 1mm, 6 mm, Picu Punch) for hydrogel, cell and media injection channels. The microfluidic chip for BSP was created using air plasma at the fixed condition of 45 sccm, 50 mTorr, 50 W, and 1 min (CUTE MPR, Femto Science, Korea), leaving behind a microfluidic channel with a flat surface for the microscale membrane. Post treatment was applied at 200 ℃, 30 min for confinement bonding properties as bonding force, bonding time.

3-2-3. Contact Angle Measurements

A drop shape analyzer (DSA-100, KRUSS) equipped with a camera was used to measure the contact angles of drops of 3 μL in volume.

3-2-4. Scanning Electron Microscope (SEM)

Images were taken using high-resolution SEM (Hitachi S4800). Samples were coated with a 2 nm Pt layer prior to analysis to prevent charging.

3-2-5. Swelling Ratio

The specimen has a diameter of 2 cm × 2 cm and a thickness of 100 micrometers. The specimen is dried in an oven at 50 ℃ for 24 h, cooled in a desiccator and immediately weighed. The test specimens are immersed in water at a cell culture temperature of 37 ℃ for 24 h, then taken out to remove water from the specimen surface and weighed immediately. The difference in weight obtained here is expressed in %.

3-2-6. Nano Indentation

The nano indentation test was taken using Nano Indenter XP (MTS, USA). The samples were fabricated in a thin film on a silicon wafer coated with a primer. The thickness of each sample was 20 ± 2 μm. The nano indenter used a berkovich diamond tip and the roundness was 40 nm. The load was pressed with a depth of 500 nm and a force of 45 mN.

3-2-7. Live/Dead Assay

The Live/Dead viability test was taken using the kit of calcein AM and ethidium homodimer-1 for mammalian cell. The media for primary cortical neuron was used neuro basal medium (NBM) with B27, GlutaMax and Peniciline-Streptomycin (Gibco, Lifetechnology). The media for human lung fibroblast (LF, Lonza) and human umbilical vein endothelial cell (HUVEC, Lonza) were used FGM-2 (Lonza) and EGM-2 (Lonza).

3-2-8 Energy-dispersive X-ray spectroscopy (EDXS)

The surface element of BSP film was analyzed at the surface of the self-detached hydrolytic cleavage. The open access microfluidic device was dipping into the deionized water in 2 days. The BSP-2 was dried at the 70 degree, 30 min. The EDXS was used X-maxN (Oxford Instrument).

3-2-9 Universal Testing Machine (UTM)

The mechanical modulus was analyzed using universal testing machine (UTM, Instron 3343). The BSP sample was fabricated 20 mm of width,

0.2 mm of thickness and 30 mm of height. The sample was dipping in the deionized water during 6 days.

3-2-10. MN-SC Coculture on a Microfluidic Chip.

All animal experiments have been conducted in accordance with protocols approved by the Institutional Animal Care and Use Committee (IACUC) at the Korea Institute of Science and Technology. As previously described, motor neuron (MNs) and Schwann cells (SCs) were cultured.[24] Briefly, MNs isolated from the spinal cord of CD-1 mice (embryonic day 13) were purified by using immunopanning dish pre-incubated with $p75^{NTR}$ antibody (Abcam) in 10 mM tris – cl solution (T& I) at 4 ℃ overnight. To culture SCs, isolated SCs from the sciatic nerves of CD-1 mice (postnatal 4) were trypsinized with a mixture of 2.5 % trypsin (Gibco) and 1mg/ml collagenase A (Roche) for 30 min. The mixture of collagen-Matrigel were loaded in the gel channels before seeding the MN and SCs on each chamber. Co culture medium consisted of neurobasal with 2 % horse serum (Thermo), 0.5 mM L-glutamine (Invitrogen), 1 % penicillin/streptomycin (P/S, Sigma), 1 mM ß-mercaptoethanol, 0.5 μM forskolin (Sigma), 0.5~2 mg/ml bovine pituitary extract, and 10 ng/ml

brain-derived neurotrophic factor (BDNF, Prospec) and changed twice a week. The experimental progress table for the PNS on chip.

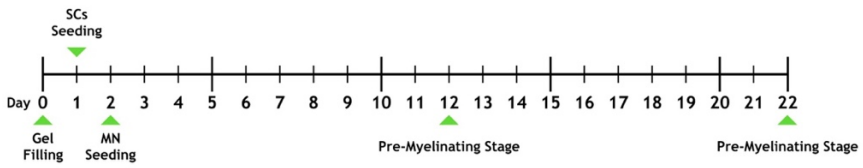

Figure. 3-3. The experimental progress table for the PNS on chip.

3-2-11. ICC: Immunocytochemistry

At DIV 20, sample was fixed with 4 % Paraformaldehyde (PFA) for 20 min and then treated with 0.1% triton x-100 for 20 min, followed by incubation with 4% BSA at 4 ° C overnight. The sample was labeled with primary antibodies, which included anti-myelin basic protein (MBP, Abcam, 1:500), anti- tubulin beta III (TuJ1, Abcam, 1:500), and DAPI (Life technologies). Secondary antibodies used were goat anti-rat IgG H&L (1:500) and goat anti-chickenIgY H&L (1:1000).

3-2-12. Western Blotting

The cells at DIV 10 and 20 were lysed in RIPA buffer (Biosesang) with protease inhibitor (Sigma). The protein concentration of cell lysates was measured by Bradford assay. The protein (4 μg) from each sample was loaded in SDS loading buffer (Bio-rad) and then transferred to a PVDF membrane (Bio-rad). The membranes were incubated with anti-MBP (Abcam, 1:1000) or anti-beta-actin (Cell signaling, 1:1000) antibodies at 4 ℃ overnight. After three 15 min washes with TBST (190 mM NaCl, 25 mM Tris, and 0.05% Tween 20, pH 7.5), membranes were incubated with anti-rat IgG-HRP (Bio-rad, 1:500) or anti- rabbit IgG- HRP (Cell

signaling, 1:1000) secondary antibodies for 1h at RT, and visualized using the Clarity Western ECL substrate (Bio-rad).

3-2-13. Cryo-Transmission Electron Microscope

Cryo-transmission electron microscope was performed at advanced analysis center at Korea Institute of Science and Technology (KIST, Korea). Briefly, cocultured samples at day *in vitro* (DIV) 10 and 20 were fixed with 4 % glutaraldehyde (Sigma) in PBS solution at 4 ℃ overnight. Following treatment with 1 % osmium tetroxide for 30 min at room temperature, samples were dehydrated in an increasingly concentrated series of ethanol solutions (70 %, 80 %, 85 %, 90 %, 95 %, 100 %), and embedded in epoxy resin. Sections were taken between 70 ~ 80 nm using ultramicrotome (Leica, Ultra Cut C), picked up on Cu grids, and stained in uranyl acetate in acetone followed by staining in lead citrate. Images were acquired with the Cryo-TEM (FEI, CryoTechnai F20)

3-3. Results and Discussion

3-3-1. Biocompatible and Self-detachable Photopolymer

The utilization of photopolymer is well adopted within the industry due to relatively fast curing speeds, nanopatterning capabilities, and high productivity by roll to roll process. In the Figure. 1b, the proposed platform investigated several formulations of various photo curable biocompatible materials for suitability. Polyethylene glycol diacrylate (PEG-DA) was used as a baseline biocompatible UV curable substrate. Trimethylolpropane triacrylate (TMPTA) and 1,6-Hexanediol diacrylate (HDDA) were investigated as UV curable substrates with potentially improved biocompatibility over PEG-DA. TMPTA is understood to possess a higher biocompatibility due to the increased crosslinking density afforded by its three acryl groups, compared to the two acryl groups and lower density in PEG-DA. HDDA, possess two acryl groups and used the competitive materials of PEG-DA. These UV curable materials (HDDA, TMPTA and Igarcure 184) were conventional pre-polymer as a raw materials of optical sheet component, such as a prism sheet, diffusion sheet of LCD light guide panel. These materials have a high cost competitive price as a point of mass production. The UV curable BSP was applied to a Si wafer for fabrication of the flat substrate, and on

a nano/micro patterned silicon master for the fabrication of the positive nano/micro patterned substrate. Thus far, PEG-DA has been the biocompatible UV curable material of choice, however, this publication has resulted in new formulations of UV curable biocompatible materials which may be more suitable.

Separation profiles were verified experimentally as shown in Figure 3-1. The OAMD was constructed in conventional closed microfluidic chip, by plasma bonding the patterned PDMS chip to the BSP substrate. Once assembled, the device was loaded conventionally with acellular and cell suspension hydrogels for three-dimensional patterning surface hydrophilicity and hydrophobicity are important factors in both plasma bonding and hydrogel patterning. This shows that the degree of modification of the hydroxyl groups of the surface can be confirmed by monitoring the change of contact angles in Figure 3-4. Contact angles were measured immediately after BSP fabrication, immediately after plasma surface treatment, and 24 h post treatment. It is important to note that the 24 h post treatment contact angle of the PEG-DA and BSP surfaces were found to be the same as that of 24 h post treatment glass. Initial contact angles were measured at around 50 degree pre-plasma treatment, and 20 to 35 degree immediately post treatment. 24 h post

treatment, contact angle recovery was measured to be 30 to 45 degrees. These trends show that PEG-DA and BSP have potential as glass substitutes in terms of hydrogel patterning related hydrophobicity. As shown in Figure 3-5, PDMS to BSP bonding strength was extensively assessed to determine whether or not the bond could survive the forces of cell patterning injection stresses. PDMS/BSP bonding strengths were found to be equivalent to that of PDMS/Glass bonds, with material failure generally occurring in the PDMS, and confirming the suitability of PDMS/BSP for cell patterning. As shown in Figure. 3-5, 1 cm diameter of PDMS/BSP area was capable of supporting a weight of 1.8 kg. The flexible linear microfluidic chip show in Figure 2b-i, as well as the three-dimensional microvessel on a chip in Figure 2b-ii demonstrates the ability to conduct substrate mechanical manipulation and deformation within a conventionally closed microfluidic platform. BSP can also be easily duplicated and patterned on a flat silicon surface by UV nanoimprinting lithography. As shown in Figure 3-6, plasma bonded PDMS with BSP-2 was confirmed FE-SEM that the interface was conformal contacted and bonded. The FE-SEM image is a cross-section of a post-designed such as a three-dimensional neuronal circuit on a chip. [72]

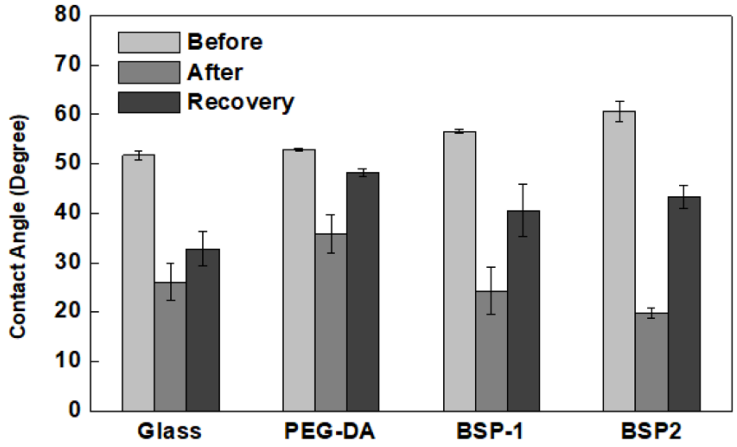

Figure. 3-4. The initial contact angle (Before) and air plasma treated surface (After) was analyzed using contact angle analysis. The waster has a similar wetting properties on the BSP surfaces. The plasma treated hydrophilic surface was recovered after 24 h. Generallay, the contact angle was increased like glass surface.

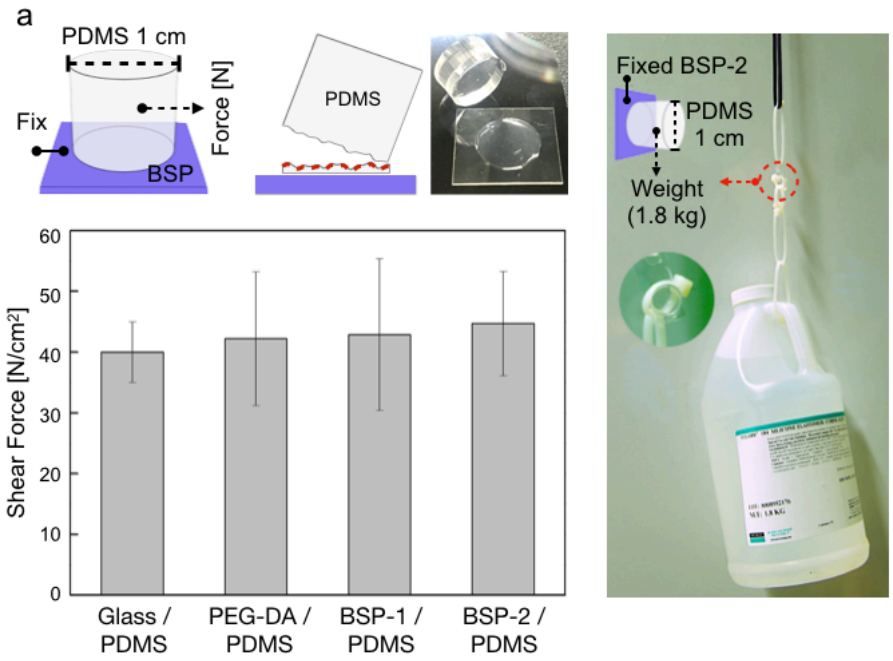

Figure. 3-5. a) The PDMS bonding strength which bonded with BSP was analyzed as a shear bonding strength test. The bonding area was a 1cm diameter slab of PDMS. The point of failure was generally in the PDMS slab, evident through the thin layer of PDMS remaining on intact BSP film. Shear bonding strength between BSP and PDMS were determined to be similar to that of PDMS and glass. The 1 cm of PDMS/BSP bonding sustain the 1.8 kg weight.

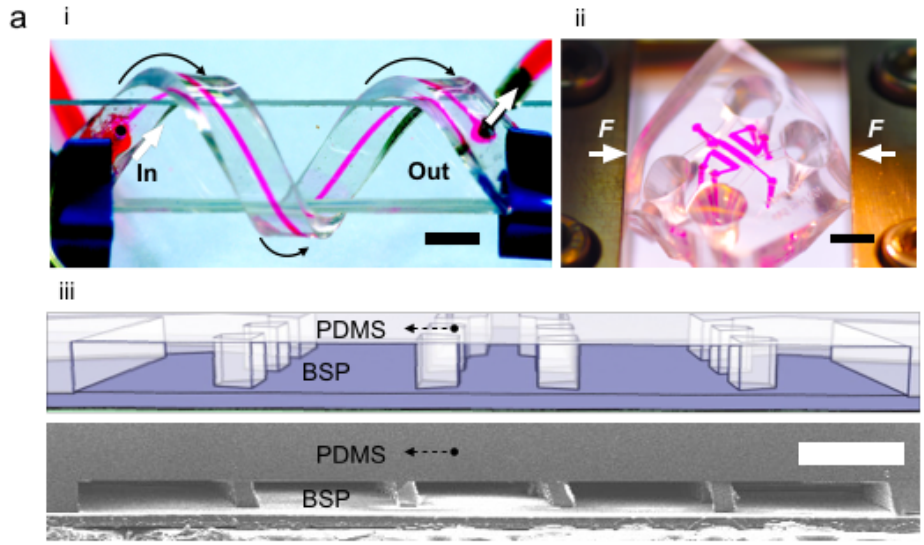

Figure. 3-6. a-i) The single channel embedded OAMD was fabricated and rolled around a glass bar and the rhodamine b solution was injected in the chip which has high flexibility. The scale bar indicates 1 cm. a-ii) The multi-channel embedded organ on a chip was bonded with BSP substrate. As compress by mechanical movement at the edge of the microfluidic chip, the tissue can be stimuli as physical bending force. The scale bar indicates 5 mm. a-iii) The upper image was a schematic illustration of the PDMS microfluidic chip bonded with BSP. The FE-SEM image was cross-section image of the micro post embedded chip for reconstitution of myelination. The scale bar indicates 800 μm.

3-3-2. Biocompatibility and Mechanical Properties

Biocompatibility for each composition was verified by viability testing with primary rat cortical neurons in two-dimensional cultures in Figure. 3-7**.** In the live/dead assays for the UV curable substrates, the following viability rates were found to be the following: 28 % for PEG-DA, 51 % for BSP-1 and 76 % for BSP-2. The observed data suggests a correlation between tri-acrylate functional groups and higher biocompatibility. Generally, the tri-acrylate group molecules have higher cross-linking densities when compared to di-acrylate group materials post UV curing. [73, 74] Interestingly, PEG-DA containing BSP-1, and PEG-DA free BSP-2 showed little difference in viability rates, while both formulations showed vast improvement over PEG-DA alone. The high degree of biocompatibility in the investigated HDDA and TMPTA formulations indicates potential as a potentially superior alternative to PEG-DA as a UV curable bioengineering materials. The substrate mechanical properties were importance function on research area of the cell differentiation, alignment, and migration. [75, 76, 77]

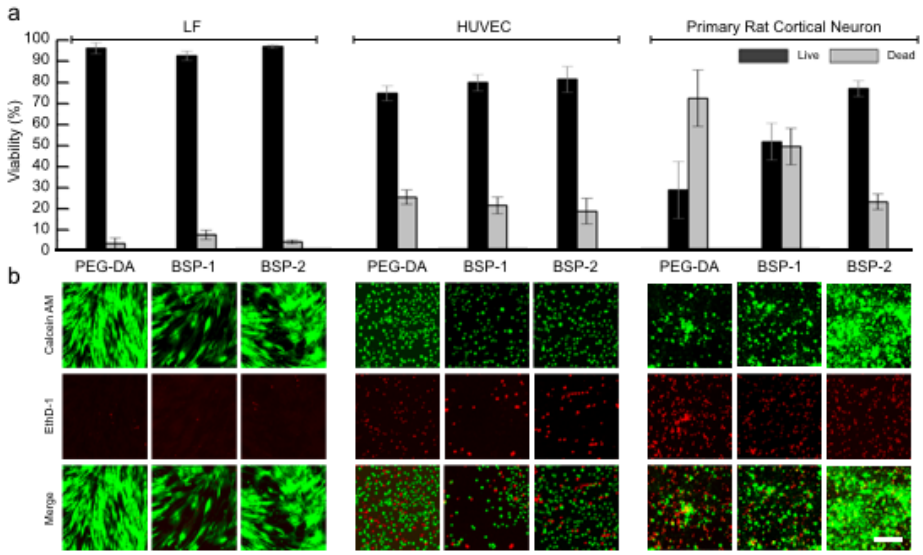

Figure 3-7. a) The Live/Dead assay of the LF, HUVEC and primary rat cortical neuron were applied on each PEG-DA and BSP-1, 2, for the biocompatibility. The BSP-2 have a high viability about the primary rat cortical neuron. b) The biocompatibility of BSP-2 was much higher than BSP-1 and PEG-DA substrate. The scale bar indicates 100 μm.

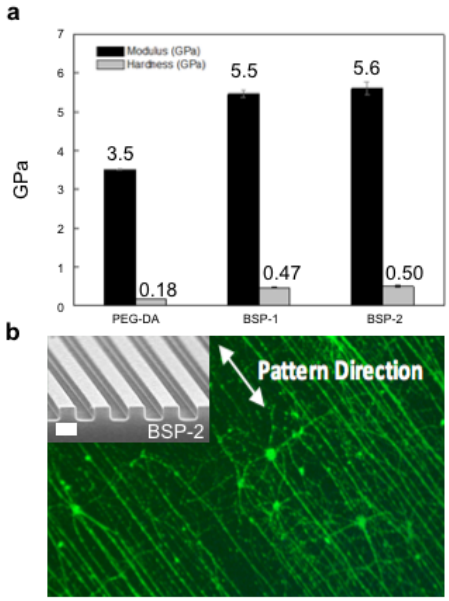

Figure 3-8. a) The BSP-1, 2 and PEG-DA have diverse mechanical properties for the two-dimensional cell culture platform. b) The BSP, UV-curable materials, was capable duplicate of nanopattern for topographical research. The FE-SEM image show the replicated nanopattern with 800 nm width and 800 nm space line patterns. The scale bar indicates 1 μm. The primary rat cortical neuron was cultured on the BSP-2 a nanopatterned surface which was coated by poly-D-lysine. The axon was well aligned with the line pattern direction. The scale bar indicates 150 μm.

As shown in Figure. 3-8, the BSP materials were measured for hardness and elastic modulus values by nanoindentation. PEG-DA (Mn 250) has relatively hard physical properties due to its relatively short molecular length. [78] BSP materials containing TMPTA have higher hardness and elastic modulus values than those without. Higher hardness is attributed to the high cross-linking density of the triacrylate group, while the overall small molecule size contributes to high elastic modulus values These values have a similar level with bone [79] surface elastic modulus values *in vivo*. Although the diverse formulations of BSP exhibited a wide range of elastic moduli, it was found that high elastic modulus has high biocompatibility which was favorable characteristic for the proposed platform. UV nanoimprinting lithography (UV-NIL) was used to nanopattern BSP surfaces, as confirmed in Figure. 3-9. Biocompatible nano patterned molds which duplicated by UV-NIL can be used for cell adhesion, directional guidance, outgrowth and accelerated outgrowth. [80] The patterned surface with a line width of 800 nm, and a space ratio of 1:1 and 1:3, 1:5 was coated in poly-D-lysine in Figure 3-10. The nanopatterned device was then used for a DIV 14 culture of primary rat cortical neurons for axonal outgrowth observation in Figure 3-10. Cellular

alignment was found to be consistent with the orientation of the 1: 5 nanopattern in Figure. 3-10.

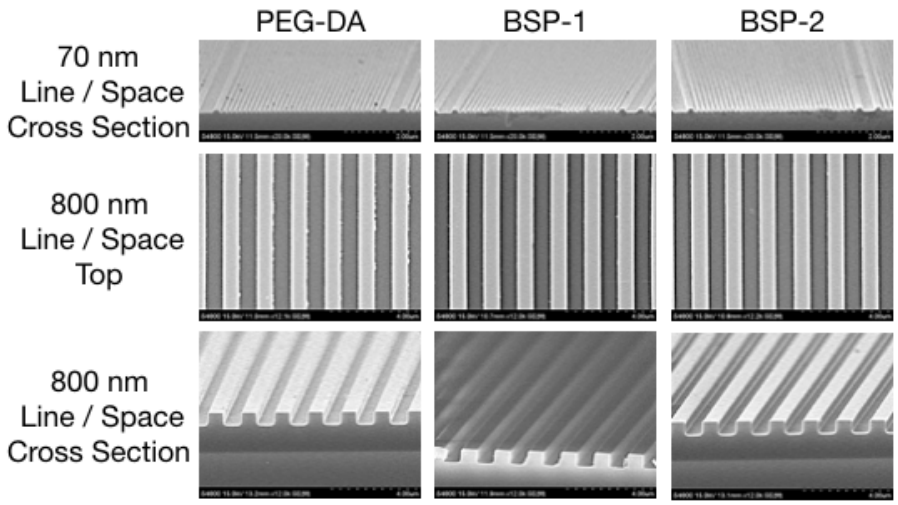

Figure 3-9. FE-SEM images of nano patterned diverse materials. All of the conditions were duplicated from the negative phase patterned silicon wafer master. These materials was duplicated up to sub 100 nm scale (70 nm line/space).

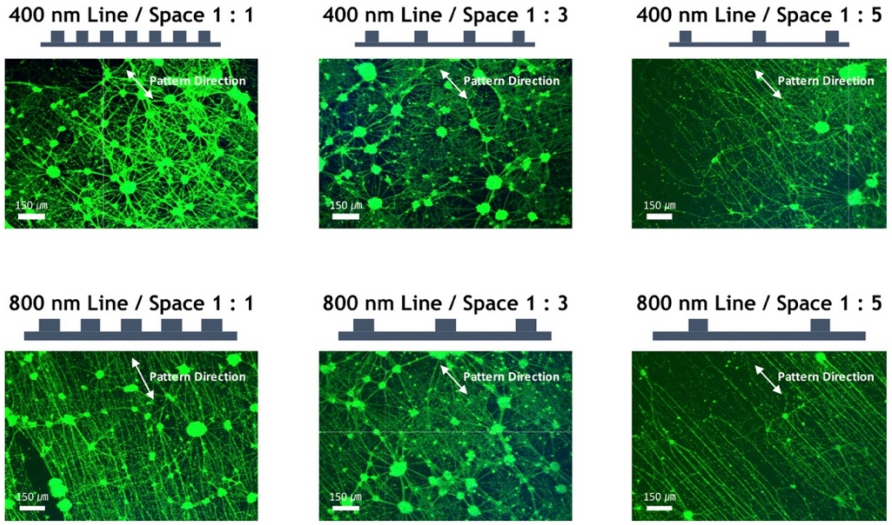

Figure 3-10. UV-NIL was carried out with BSP-2 material. Line width of 400 nm and 800 nm, and a space ratio of 1 : 1, 1 : 3, 1 : 5. The surface was coated with PDL and cells were cultured. On top of this, primary cortical neurons were cultured for 2 weeks to observe how the axons outgrowth. We could confirm the outgrowth consistent with the orientation of the nanopattern in the 1: 5 line / space pattern. Such low viability cells need to be studied with higher biocompatibility polymers. The primary cortical neuron was plated 0.1 mil/ml in 4 cm^2 area.

3-3-3. Self-detachable for Open-access Organ on a Chip

As shown in Figure. 3-11a, the schematic illustration of the OAMD was presented. The substrate was optically transparent film, and self-detached from the PDMS microfluidic device. The interface, which was plasma bonded PDMS with BSP-2, was spontaneously separated by hydrolysis cleavage. In Figure 3-4 which was shown the bonding strength analysis, before the water absorption, the mechanical failure was shown the PDMS cohesive area. The other way, during the tissue culture on the OAMD, the cell culture media was spontaneous infiltrate the plasma bonded interface. After the hydrolysis cleavage of the bonded interfaces, the BSP film was not shown any residue material such as the Matrigel and collagen which was injected into OAMD. This is the strong point for the without structure damages sampling of the for the TEM analysis. The PEG-DA and BSP have the self-detachable characteristic which was used as substrate materials on a microfluidic device. The self-detachable properties, as mentioned before, was induced by the water absorption characteristic. In Figure 3-11b, the glass did not show the water absorption property, but the PEG-DA and BSP materials showed the water absorption properties. The 5% of PEG-DA, 3 % of BSP-1 and 2.5 % of BSP-2 were shown using the DI water swelling ratio test. The cell culture on the OAMD, the

substrate was self-detached after 2 days when using the PEG-DA. And the BSP materials were shows that 1 day of BSP-1 and 12 h of BSP-2 in Figure. 3-11c. The separation area was spontaneously increased and finally, the whole BSP film was totally separated after 2 days. The Different combinations of substrate materials can be employed to modulate the separation rates between the base and the main device. The self-detachable film was generated by hydrolytic cleavage by hydrolysis reaction at the carboxylate ester group which was the native chemical structure of the BSP resin molecule. Generally, PDMS and organic substrate bonding interface are vulnerable to the hydrolysis reaction. Especially, the carboxylate ester group was vulnerable to the hydrolytic cleavage. In Figure 3-12, using the PEG-DA, HDDA and TMPTA as the raw materials of substrate which obtained the carboxylate ester group natively. The PEGDA and HDDA had a two-carboxylate ester group and the TMPTA has a three-carboxylate ester group. These materials mean chemically unstable structure at the hydrolytic reaction. In Figure 3-13, the self-detached BSP surface, which was bonded with PDMS area, was analyzed using energy-dispersive X-ray spectroscopy (EDXS) for the confirm the self-detachable photopolymer system.

If the hydrolytic cleavage was generated in the PDMS area, the BSP surface was obtained the Si atoms. But the BSP surface was not detected the Si atoms. This means the hydrolytic cleavage was generated in the BSP area. Also, the cleavage of the open access microfluidic device (OAMD) was generated only wet condition. In Figure 3-14, the mechanical modulus of the wet conditioned BSP was decreased versus dry conditioned BSP. The decrease of the mechanical property was the proof of the hydrolysis reaction was generated in the BSP film. PEGDA, HDDA and TMPTA all materials were vulnerable to the hydrolytic reaction.

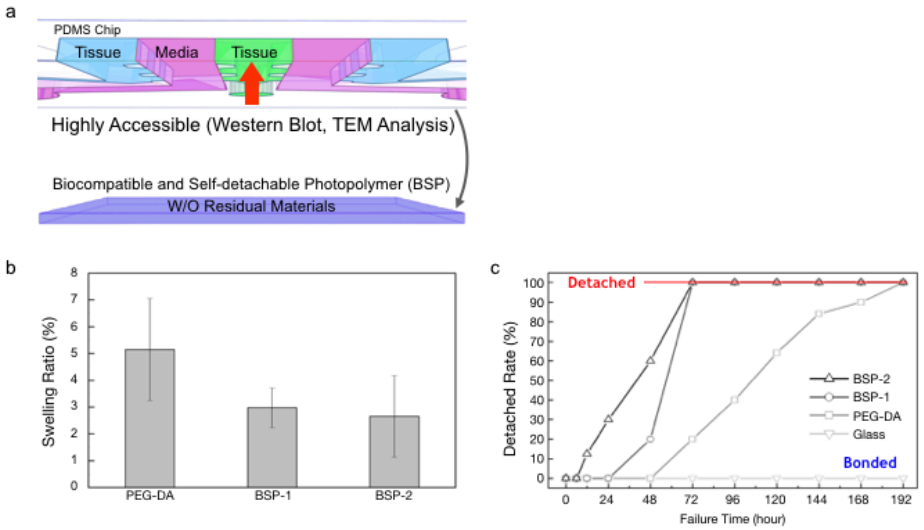

Figure. 3-11. a) The schematic illustration of spontaneous detachment for BSP integrated open-access microfluidic chip. The BSP was smoothly detached without any tissue residue on the surface. b) The swelling ratio was analyzed for the spontaneous detachment of BSP. The PEG-DA and BSP have swelling property compared with a glass substrate. c) The PEG-DA was bonded 48 h, and BSP-1, 2 were bonded 24 h, 6h in the aqueous medium solution which was bonded 1 cm diameter PDMS slab. The bonding area was gradually decreased.

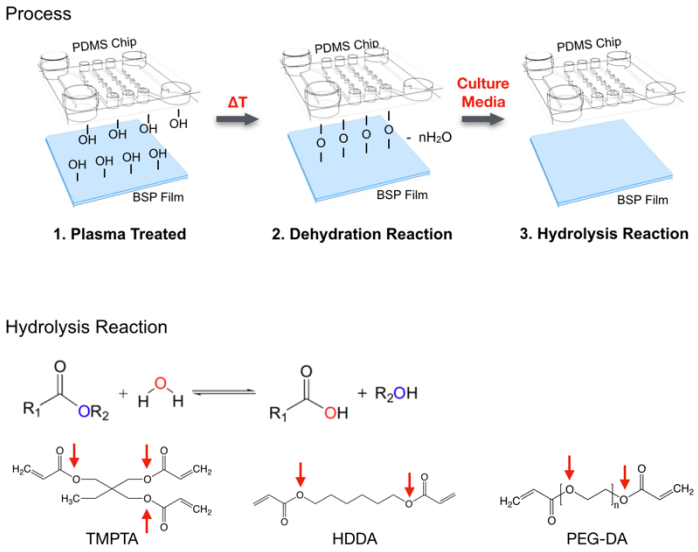

Figure. 3-12. The illustration of the open access microfluidic device. The self-detachable film was generated by hydrolytic cleavage by hydrolysis reaction at the carboxylate ester group which was the native chemical structure of the BSP resin molecule.

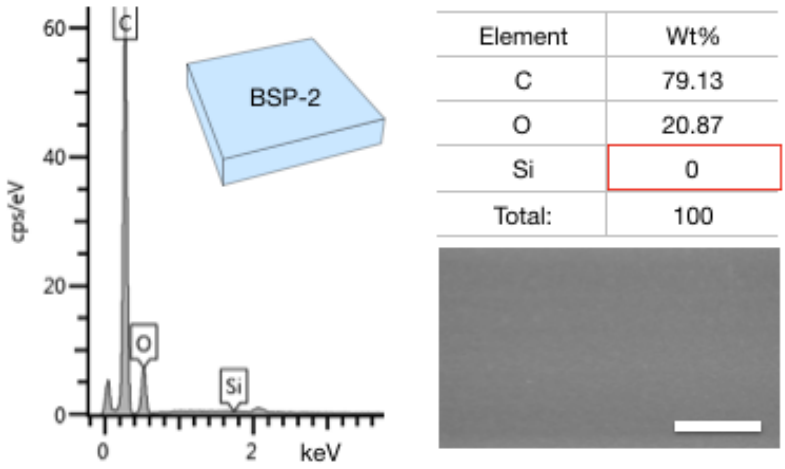

Figure. 3-13. The open access microfluidic device was separated at the self-detached BSP film. The Si atom was not detected on the BSP film using energy-dispersive X-ray spectroscopy (EDXS) analysis.

	Condition 1	Condition 2
Dry	O	X
Wet	X	O
Device Separation	X	O

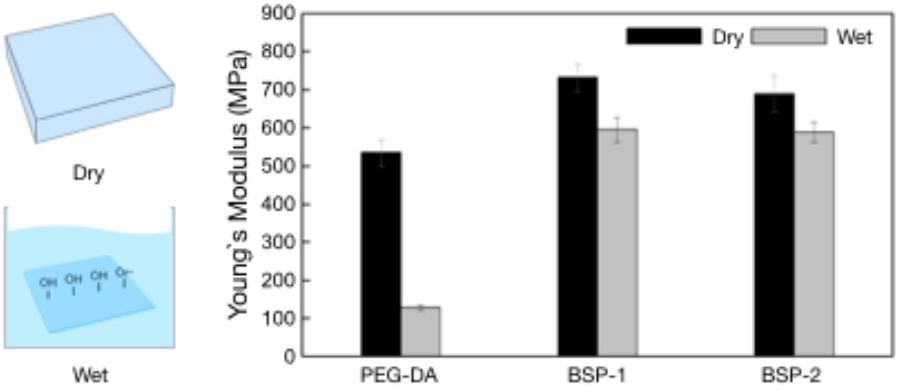

Figure. 3-14. The cleavage of the open access microfluidic device (OAMD) was generated only wet condition. The mechanical modulus was decreased in the wet condition which was the hydrolysis reaction generated.

We examined the formation of the myelin sheath in the PNS model, by analyzing myelin basic protein (MBP) expression. At DIV 20, MBP expression was checked confocal microscopy in Figure 3-15. The myelinating stage at DIV 20, MBP expression appeared to be highly localized along the motor neuron axon which was demonstrated the myelinating stages in 2-D coculture. In the two-dimensional coculture, myelination initiated by migration of SCs toward axons was classified into the two distinct stages on the basis of the MBP expression pattern in the myelinating SCs process. The pre-myelinating stage was diffused of SCs toward around the MN axons, and the myelinating stage was the well-defined along the axons by progress to a tightly localized. Also, the myelin basic protein (MBP) and beta-actin expression were confirmed by western blot by the BSP-2 used OAMD in Figure 3-15. As shown in Figure 3-16, pre-myelination was confirmed at DIV 10 and complete myelination at DIV 20 for the thickness of myelin sheath using the transmission electron microscope (TEM). TEM imaging was made possible by the nondestructive open-access of the cultured tissues via the BSP. As shown in Figure 3-16, the myelin structure was analyzed as high precision which was cultured on the microfluidic chip of PNS. As demonstrated, the OAMD is capable of highly specialized and controlled microfluidic cell

culture, as well as the ability to allow for nondestructive tissue collection for detailed imaging. OAMD techniques can be further applied to many other microfluidic cell culture schemes to allow detailed imaging and sampling techniques that have been previously impossible due to the closed nature of conventional microfluidic systems.

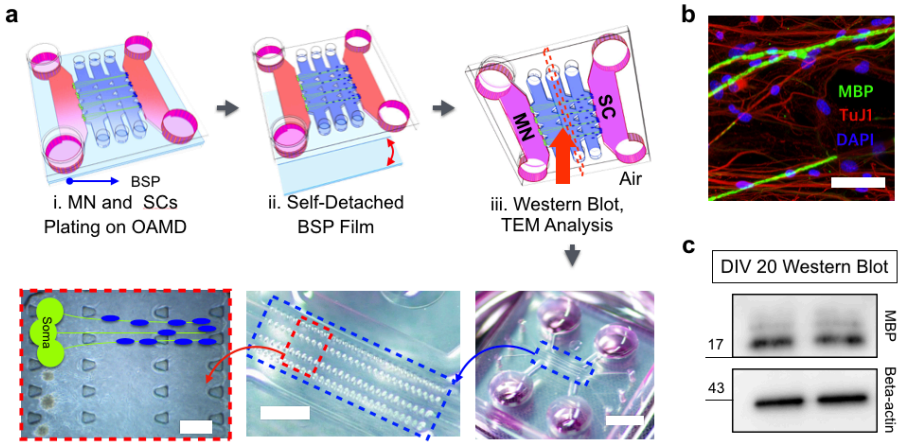

Figure 3-15. a) The illustration of peripheral nervous system (PNS) myelin structure composed by MN and SCs. The SCs was myelinated on the MN axon. The three-dimensional myelin structured tissue was open to the air without any coverage materials. The inset image was showed the whole chip of open-access microfluidic chip after tissue culture. The scale bar indicates 2 mm. The microscope image was showed the motor neuron (left) and Schwann cell (right). The scale bar indicates 500 μm. b) The immunocytochemistry was applied for the MBP and TuJ1 expression about the myelination. c) The myelin basic protein and beta-actin were confirmed by western blot.

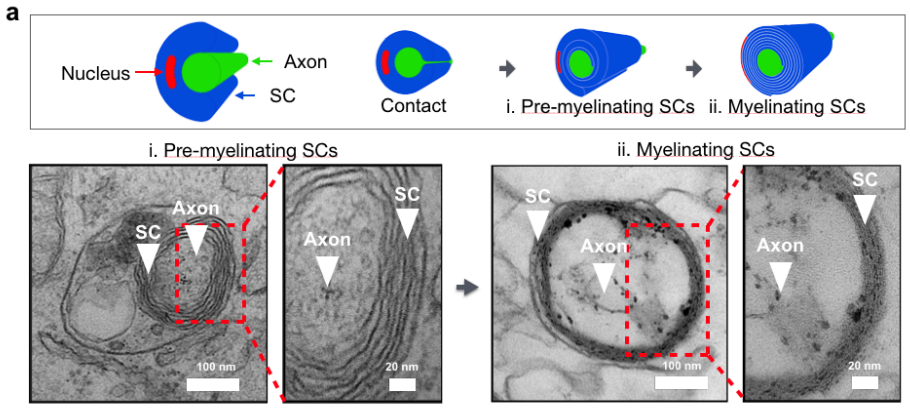

Figure 3-16. a) TEM imaging verified pre-myelinating SCs by DIV 10, and complete myelinating SCs by DIV 20. The left image scale bar indicates 100 nm and scale bar of the magnified image indicates 20 nm. This accessibility of BSP integrated open-access microfluidic chip was able to confirm the structure of *in vitro* mimic tissue.

3-4. Conclusion

This publication proposed the use of HDDA and TMPTA as biocompatible and self-detachable photopolymers (BSP) as a substrate for the proposed open-access microfluidic device (OAMD) platform. The ability of the OAMD platform to allow for the non-destructive sampling of cultivated tissues allows for previously impossible. BSP as the UV curable materials can be utilized as transparent, flexible and nano patternable substrates for topographical cell behavior research through UV nanoimprinting lithography (UV-NIL). The BSP can be plasma bonded to PDMS and possesses strong bonding strengths similar to those of glass. Biocompatibility of the BSP was verified by the live/dead assay of primary rat cortical neurons in two-dimensional culture, and three-dimensional reconstituted PNS tissue. BSP shows a higher water absorption rate compared to that of conventional glass. Consequently, the self-detachment of BSP from PDMS occurs spontaneously over the course of the cell culture. Myelination was confirmed via western blot and TEM through non-destructive OAMD sampling. The direct and nondestructive accessibility of OAMD culture systems through the use of BSP shows great promise in any research applications which require direct tissue sampling and high accessibility for structural analysis.

Chapter 4

Vascularized tissue transplantation from open-access microfluidic device for regenerative therapy of PAD

4-1. Introduction

As show in Figure 4-1, for develop safe and effective procedures for vascularized tissue injection, we focused on regenerative medicine technology using “Open microfluidic device”. Vascularized Tissue (VT) formation is a well-known process associated with microvessel culture processes, and using microfluidic device with several advantageous features for organ on a chip. For example, the VT has a 3-D structure that may provide a rich extracellular matrix that is more relevant to the *in vivo* environment. Furthermore, VT can be defined to form certain microstructure. We herein report a novel open microfluidic device that yields functional and vascularized tissue that can be successfully transplanted into the Balb C Nu nude mouse.

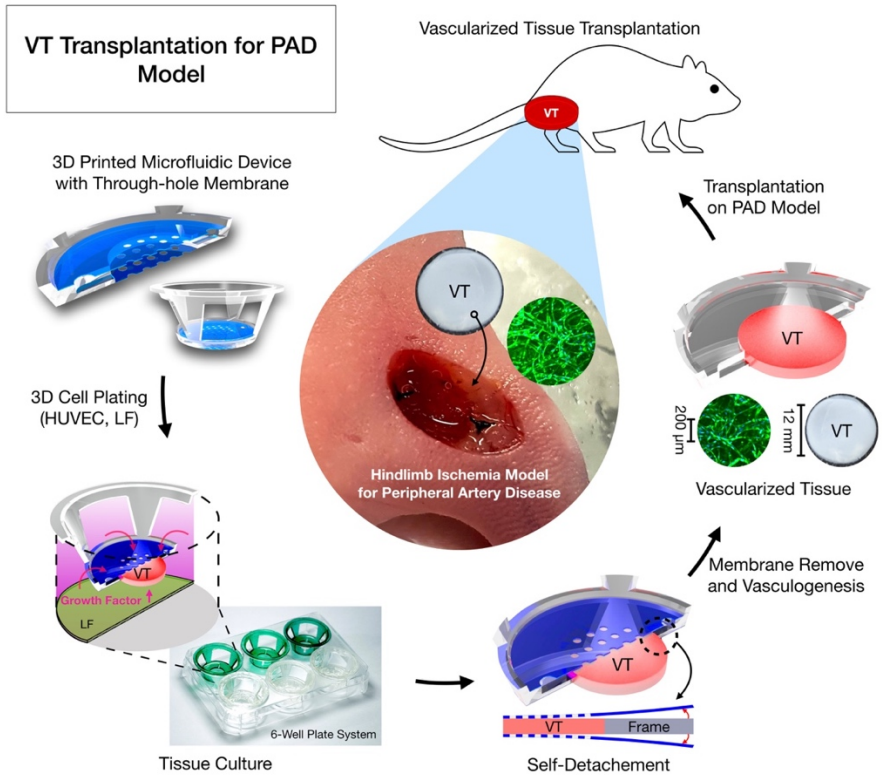

Figure 4-1. Schematic of fabrication of VT transplantation for PAD model. Double side through-hole membrane was integrated 3D printed microfluidic device. The transplantable microfluidic device was culture as a 6-well plate culture system. During the culture of the vascularized tissue, plasma bonded PEG-DA through-hole membrane was spontaneously detached by water absorption of the culture media. The VT was transplanted to the hindlimb ischemia model as a regenerative medicine.

4-2. Materials and Method

4-2-1. 3D Printed Microfluidic Device

The 3D printed microfluidic device was used the stereolithography apparatus (SLA) and digital light process (DLP) system. The Projet® 1200 Micro-SLA printer was used as the commercially available for the easily assembled 3D printed microfluidic device. The photoresin was used the Visijet® FTX Green (3D SYSTEMS, USA) which used for micro-fine detail casting patterns and plastic parts with dark green color. The Projet® 1200 Micro-SLA has a 56 μm (585 dpi) of XY resolution and 30 μm of Z layer resolution. And, the LITHO® (Illuminaid, Korea) used for the custom 3D printing of PEGDA photoresin which has a biocompatibility and transparency. LITHO has 82 μm of XY resolution and from 25 μm to 200 μm of Z layer resolution. Figure 4-2 was show the schematic illustration of the 3D printed microfluidic device and the integrated on the 6-well plate system.

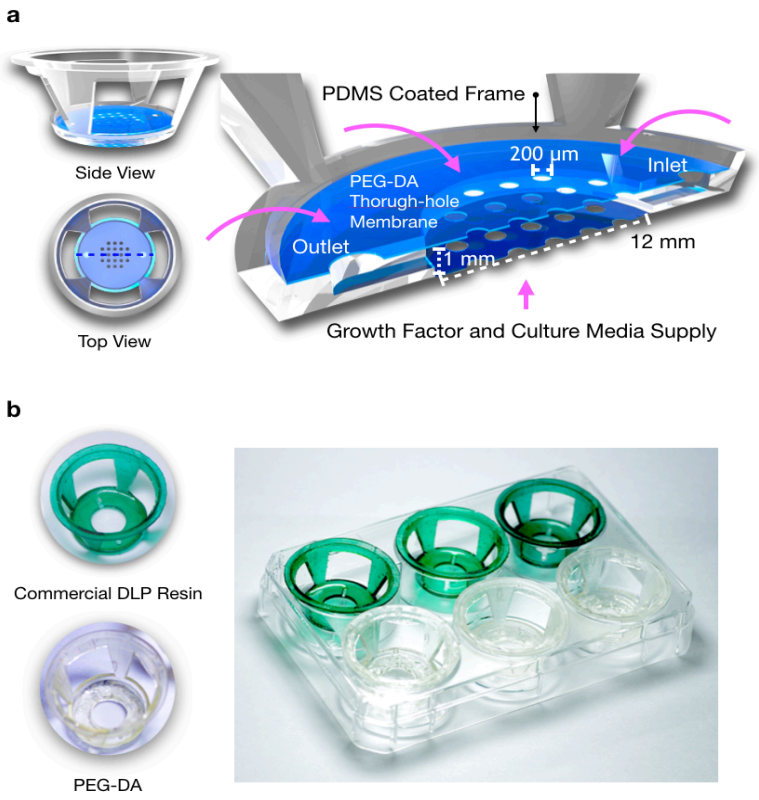

Figure 4-2. a) The side and top view images were shows as use of the insert part which made by the 3D printing technology. Cross-sectional image of 3D Microfluidic device. The top and bottom materials were composed as PEG-DA photoresin which has a 200 µm diameter through-hole membrane. b) The green colored insert part was printed using commercial UV curable resin using commercial 3D printer. The clear insert part was printed customized 3D printer with customized PEG-DA resin.

4-2-2. Photoresin Preparation

The PEG-DA resin were fabricated using the UV replica molding method in which PEG-DA UV curable solution was mixed with 97 wt% (by mass) of Polyethylene glycol diacrylate (PEG-DA, Mn 250, Sigma-Aldrich, viscosity 15 ~ 35 cP) pre-polymer with 3 wt% of 1-hydroxy-cyclohexyl-phenyl-ketone (Irgarcure 184, BASF) as photo-initiator. All these steps were done in the dark to avoid spontaneous reaction with ambient light.

4-2-3. Surface Treatment

Parylene C deposition on 3D printed microfluidic device was performed with a commercially available parylene coater (LAVIDA, FEMTO SCIENCE). Temperatures used for vaporization, pyrolysis and deposition of parylenes were 680 ◦C and room temperature. Vaporized parylene-monomers attached the 3D printed microfluidic device. After the parylene coating process, the PDMS thin layer was coated on the microfluidic cell loaded area for the plasma bonding with PEG-DA through-hole membrane. The microfluidic channel was dip coated using mixture of PDMS prepolymer. The thickness of the coated PDMS layer was 10 ~ 20

μm. This interface PDMS PEG-DA through-hole membrane which was supplied the open-access microphysiological system.

4-2-4. Through-hole Membrane Integration

The membrane was fabricated in three simple steps. The first step combines plasma bonding of the top part of a PDMS microfluidic chip with a flat substrate. The microfluidic chip for the through-hole membrane was created using air plasma under fixed conditions of 45 sccm, 50 mTorr, 50 W, and 1 min (CUTE MPR, Femto Science, Korea), leaving behind a microfluidic channel with a flat surface for the microscale membrane. The second step was curing of membrane materials, the chip was exposed to UV light for 180 s (UV wavelength = 250–400 nm, dose = 100 mJ cm^{-2}). The third step is separating the membrane by mechanical failure, using a scalpel and mechanical force. The PDMS microfluidic chip edge was severed using a scalpel and the micro/nanopillar substrate was separated by cohesive mechanical failure on the bottom surface after curing. The experimental through-hole membrane was fabricated by applying the pre-polymer membrane material through a PDMS microfluidic chip patterned with distribution channels into a mold. For microscale membrane production, the PDMS microfluidic pre-polymer distribution chip is also

patterned with positive micropillars (diameter 200 μm) and plasma bonded to a flat surface backer, like glass. Post injection, the assemblies are cured and then the membranes are mechanically extracted for use. The negative micropillar patterned master was fabricated using a conventional lithography process with SU-8 photoresist (SU-8100, MicroChem, USA) for the positive micropillar patterned microfluidic chip. The mold was replicated from the negative patterned SU-8 master using PDMS (Sylgard 184, Dow Corning, USA). The comparatively large inlet/outlet ports were punched via 1 mm medical grade skin biopsy punch (diameter 1 mm, Picu Punch) for membrane material injection channels.

4-2-5. Cell Culture and Vasculogenesis Cell Seeding

Human umbilical vein endothelial cells (HUVEC, Lonza) were cultured in Endothelial Growth Medium (EGM-2, Lonza) and passages 5 to 7 used for experiments. Normal human lung fibroblasts (LF, Lonza) were cultured up to passage 10 in Fibroblast Growth Medium (FGM-2, Lonza). Cell cultures were grown to 80% confluence prior to passage or use in experiments. All cells were maintained in a humidified incubator at 37 uC and 5 % CO_2. The fibrinogen solution was prepared by dissolving 2.5

mg/ml bovine fibrinogen (Sigma) in DPBS (Gibco) and supplementing aprotinin (0.15 U/ml, Sigma) and collagen type I (0.2 mg /ml, BD bioscience) to the solution. Collagen type I was added to the pure fibrin matrix to enhance lumen formation of developing tubular structures. After disassociation from culture dishes using 0.25% Trypsin-EDTA (Hyclone), HUVECs and LFs were suspended in the fibrinogen solution, at a concentration of 5×10^6 cells/ml for HUVECs and 5×10^6 cells /ml for LFs. The cell solutions were mixed with thrombin (0.5 U/ml, Sigma) and then immediately injected into a microfluidic channel and substrate of 6 well plate. The 6-well of the cell culture medium were loaded with EGM-2 medium. Following loading the 6-well plate as showed in Figure 4-3, the microfluidic platforms were incubated at 37 ℃ and 5% CO_2. The cell culture medium was removed and refilled with fresh EGM-2 culture medium every 48 h.

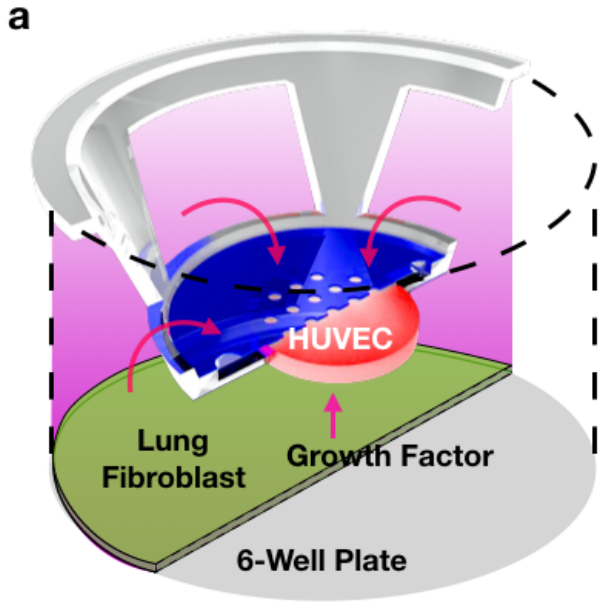

Figure 4-3. Schematic illustration of the tissue culture platform using 6-well plate system. The bottom layer was coated by lung fibroblast for growth factor supply.

4-2-6. Immunostaining and Imaging

Mouse monoclonal antibodies specific for CD31 (Alexa Fluor1647, clone WM59) was purchased from BioLegend. Mouse monoclonal antibody specific for Hoechst 33342 was from Molecular Probes. After washing cultures once with phosphate-buffered saline (PBS, Hyclone), cells were fixed in 4% (w/v) paraformaldehyde in PBS for 30 min. After blocking using 3% bovine serum albumin (BSA, Sigma) in PBS for 1 h, samples were incubated overnight at 4 uC either with primary antibodies directly conjugated with fluorescent marker (CD31; 1 : 200). For staining nuclei, Hoechst 33342 (1 : 1000) were added to the chip for 1 h of incubation at room temperature. The samples were washed three times and stored in PBS before imaging. For cross-section and whole-construct imaging of 3D blood vessels, stained samples were examined using a FluoView FV1000 confocal laser scanning unit with the IX81 inverted microscope (Olympus) and images were captured with a confocal PMT detector. Lenses in use were ×10, ×20 and ×40 (Olympus). Confocal images were processed by IMARIS software (Bitplane).

4-2-7. Hindlimb Ischemia Model and in vivo Vascularized Hydrogel Implantation.

All animal experiments were performed using protocols approved by the Seoul National University Institutional Animal Care and Use Committees. BALB/C-nu mice (female, age 6 weeks, weighing 20~25 g) were purchased from Orient Bio (Orient Bio Inc, Seongnam, Korea). All mice were anesthetized with an intraperitoneal injection of Zoletile 50 (Tiletamine + Zolazepam, 0.006 ml/10g) and Rompun (Xylazine, 0.004 ml/10g) and the inguinal skin was incised along with the femoral artery visible through the skin. The femoral artery was excised from its proximal origin as a branch of the external iliac artery to the distal point where it bifurcates into the saphenous and popliteal arteries. After femoral artery excision, the mice was treated with PBS (400 μl, Control group), hydrogel (Gel group), HUVEC (5 million cells re-suspended with 400 μl of PBS, Cell group), HUVECs mixed hydrogel (5million cells re-suspended with 400 μl of hydrogel, Cell + Gel group) and Vacularized hydrogel disk (400 μl of hydrogel was vascularized with 5 million HUVECs, Vascularized hydrogel group). Blood flow of hindlimb was measured via a laser Doppler perfusion imaging (LDPI) analyzer (Moor instruments, Devon, UK) on days 0, 7, 14, 21, and 28 after sample insertion. The degree of

blood perfusion was calculated on the basis of colored histogram pixels. Blood perfusion is expressed as the LDPI index indicating the ratio of ischemic versus non-ischemic limb blood flow. The scores of necrosis in the ischemic hindlimb were assessed on day 28 after surgery (0: salvage of limb, 1: toes amputation, 2: foot amputation, 3: limb amputation).

4-2-8. Histological Analysis and Immunostaining

For histological evaluation, muscle tissues of hind limb were isolated and fixed with paraformaldehyde (4% PFA). The day after, tissues were placed in 20 w/v% sucrose in PBS for overnight at 4℃. Then, tissues were transferred into OCT compound (Tussue-Tek®) and 20 w/v% sucrose in PBS mixed solution (OCT compound: 20 w/v% sucrose in PBS = 1 : 1 volume ratio). After two hours, the samples were placed in the cryo-mold and the cyro-mold was filled with OCT compound. Tissue embedded cryo-mold was solidified in isopentane solution chilled by liquid nitrogen and the frozen tissue block was sectioned using cryostat (thickness = 10 μm). The tissue sections were immunostained with CD31 (endothelial cell marker, 550274, BD Biosciences) and α-smooth muscle actin (smooth muscle cell marker, ab5694, Abcam) primary antibodies. The samples were incubated with Alexa Fluor 488 goat anti–rat or Alexa Fluor 594

goat anti-rabbit secondary antibody (Life Technologies) and the nuclei were counterstained with 4',6 – diamidino-2-phenylindole (DAPI).

4-2-9. Self-detachable for Advanced Analysis of Organ on a Chip

As shown in Figure. 4a, c, the schematic illustration of the VT was presented. The substrate was optically transparent film, and self-detached from the PDMS microfluidic device. The interface, which was plasma bonded PDMS with BSP-2, was spontaneously separated by hydrolysis cleavage. In Figure. 2a which was shown the bonding strength analysis, before the water absorption, the mechanical failure was shown the PDMS cohesive area. The other way, during the tissue culture on the OAMD, the cell culture media was spontaneous infiltrate the plasma bonded interface. After the hydrolysis cleavage of the bonded interfaces, the BSP film was not shown any residue material such as the Matrigel and collagen which was injected into OAMD. This is the strong point for the without structure damages sampling of the for the TEM analysis. The PEG-DA and BSP have the self-detachable characteristic which was used as substrate materials on a microfluidic device. The self-detachable properties, as mentioned before, was induced by the water absorption characteristic. In

Figure. 4b, the glass did not show the water absorption property, but the PEG-DA and BSP materials showed the water absorption properties. The 5% of PEG-DA, 3 % of BSP-1 and 2.5 % of BSP-2 were shown using the DI water swelling ratio test. The cell culture on the OAMD, the substrate was self-detached after 2 days when using the PEG-DA. And the BSP materials were shows that 1 day of BSP-1 and 12 h of BSP-2 in Figure. 4c. The separation area was spontaneously increased and finally, the whole BSP film was totally separated after 2 days. The Different combinations of substrate materials can be employed to modulate the separation rates between the base and the main device. Figure. 5a shows that the PNS chip was segregated into two chambers by a collagen-Matrigel mixture hydrogel, with motor neurons on one side and Schwann cells on the other. The myelin structure was reconstituted on the microfluidic devices in Figure. 5a. The specific experiment progress table was shown in Figure. S4. We examined the formation of the myelin sheath in the PNS model, by analyzing myelin basic protein (MBP) expression. At DIV 20, MBP expression was checked confocal microscopy in Figure. 5b. The myelinating stage at DIV 20, MBP expression appeared to be highly localized along the motor neuron axon which was demonstrated the myelinating stages in 2-D coculture.[24] In the two-dimensional

coculture, myelination initiated by migration of SCs toward axons was classified into the two distinct stages on the basis of the MBP expression pattern in the myelinating SCs process. The pre-myelinating stage was diffused of SCs toward around the MN axons, and the myelinating stage was the well-defined along the axons by progress to a tightly localized. Also, the myelin basic protein (MBP) and beta-actin expression were confirmed by western blot by the BSP-2 used OAMD in Figure. 5c. As shown in Figure. 5d, pre-myelination was confirmed at DIV 10 and complete myelination at DIV 20 for the thickness of myelin sheath using the transmission electron microscope (TEM). TEM imaging was made possible by the nondestructive open-access of the cultured tissues via the BSP. As shown in Figure. 5d, the myelin structure was analyzed as high precision which was cultured on the microfluidic chip of PNS. As demonstrated, the OAMD is capable of highly specialized and controlled microfluidic cell culture, as well as the ability to allow for nondestructive tissue collection for detailed imaging. OAMD techniques can be further applied to many other microfluidic cell culture schemes to allow detailed imaging and sampling techniques that have been previously impossible due to the closed nature of conventional microfluidic systems.

4-3. Results and Discussion

4-3-1. Vascularized Tissue Process and Self-detached Through-hole Membrane

The experimental process was shown in Figure 4-4. First, the vascularized tissue (VT) was cultured on the 3D printed microfluidic device. Total culture time was day 14. The vascularized tissue was well obtained without any physical damages by self-detached through-hole membrane as mentioned before. For the VT, the through-hole membrane was plasma bonded until 4 days maximally and then, the membrane was spontaneously detached. The plasma bonding strength appeared bonding temperature dependent. Generally, the plasma bonding temperature was applied under hundred degree. But for the PEG-DA, the bonding temperature was not enough to the high bonding strength as shown in Figure 4-5a. For the PEG-DA membrane bonding, the temperature was applied two hundred degree and different time applied as 5 min, 30 min, 60 min. As showed graph in Figure 4-5a, 5 days bonding strength was appeared by at the condition of two hundred degree and 30 min. After the detached through-hole, the vascularized tissue was obtained without any physical damages for transplantation.

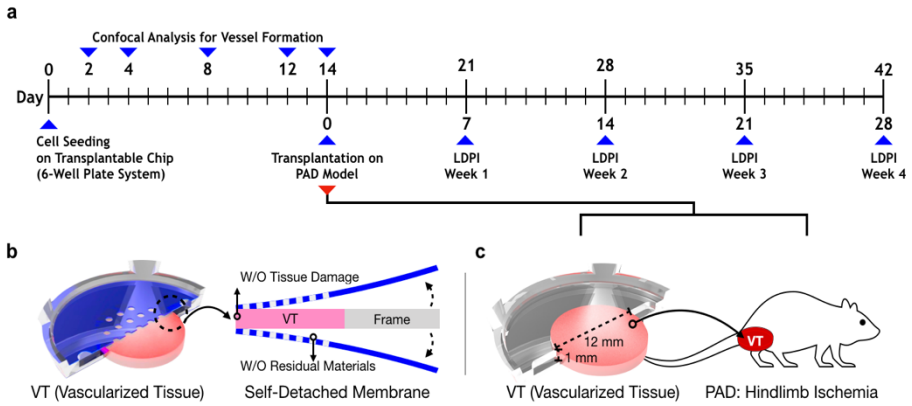

Figure 4-4. a) The experimental progress table for the PAD regenerative mediciene. b) The thorough-hole membrane was spontaneously self-detached by water absorption of the culture media. c) The VT was transplanted on the hindlimb ischemia after 14 days cultured.

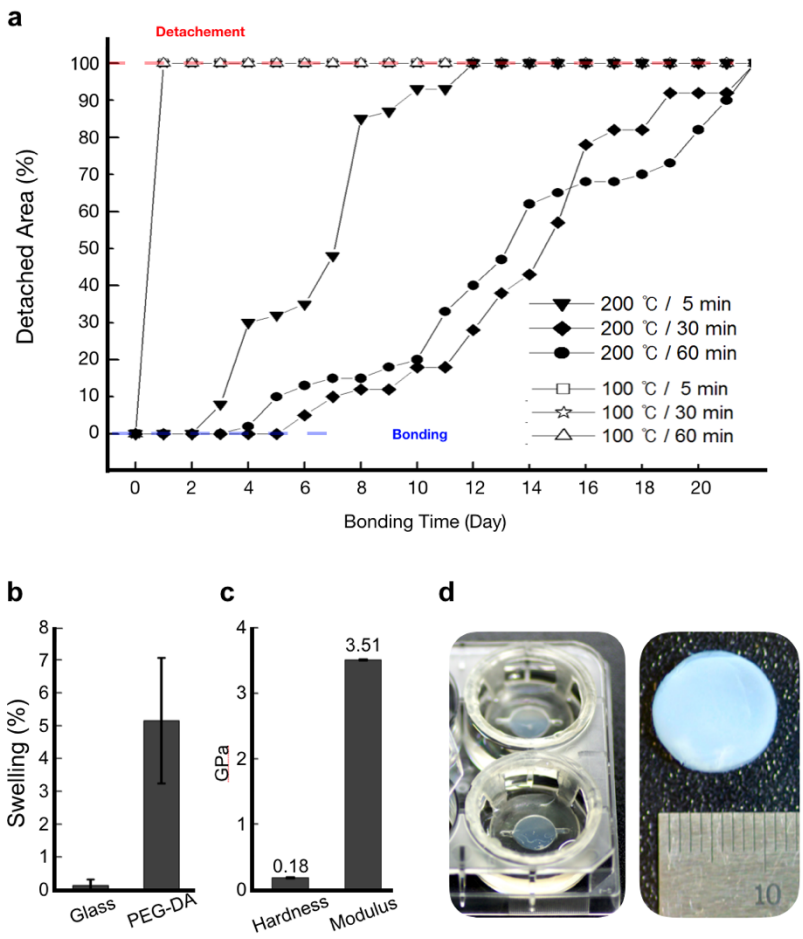

Figure 4-5. a) The PEG-DA has high water absorption properties than glass. b) The PEG-DA show the high mechanical properties for the surface topographical study. c) Self-detached propertie was showed as spontaneously separation by hydrolysis reaction. d) The vascularized tissue (VT) was cultured on well plate and the right image was show the diameter of VT.

4-3-2. Vascularized Tissue Analysis

We analyze the growth of the HUVEC microvessel network and angiogenic sprouts as it occurred over several days. We used human umbilical vein endothelial cells (HUVECs) as vascular precursor cells, and human normal lung fibroblasts (LFs) as stromal cells to support HUVEC morphogenesis via secretion of pro-angiogenic growth factors and extracellular matrix proteins.[27,28] To recreate highly pro-angiogenic ECM environments as found in wound healing and solid tumors,[29] we supplemented fibrin matrix with type I collagen (referred to simply as ‘‘fibrin matrix’’ hereafter) to form ECM constructs. A day after seeding, HUVECs displayed elongated morphology with appearance of intracellular vacuoles in Figure 4-6. Assembly of HUVECs into tubule-like structures encompassing a nascent lumen was observed as early as day 2. Further development of the vasculature resulted in interconnected networks occupying extended areas of fibrin matrix after 3 days. Perfusable microvascular networks that can be directly accessed via fluidic channels were established by day 10 to 14.

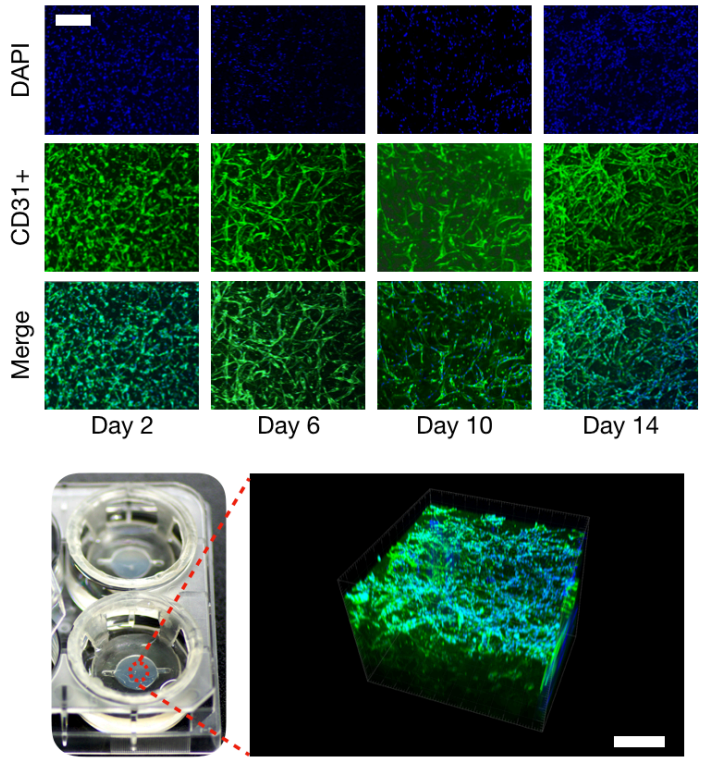

Figure 4-6. Time-series micrographs of vasculogenic vessel formation in the fibrin matrix. Day 2, HUVECs elongate and start to connect to each other. Day 6, HUVECs start to form a network via a dynamic remodeling process, while nascent lumen structures appear. By Day 10, hollow lumina of HUVECs grow larger and merge to form well-interconnected tubular structures. By Day 14, a perfusable microvascular network is established as the luminal sides of the vessels are connected. The lower imager was show the 3D microvessel image at Day 14. The scale bar indicates 200 μm and 300 μm

4-3-3. Vascularized Tissue improves recovery of blood perfusion and limb salvage in an ischemic hind limb.

To evaluate the angiogenic efficacy of vascularized hydrogel in hind limb ischemia model, the recovery of blood perfusion and salvage of ischemic tissue were assessed using several experiments in BALB/c mice. The amount of blood flow was measured using a laser Doppler perfusion imaging (LDPI) analyzer during four weeks with injections and implantation of 5 groups (1. Control: PBS, 2. Gel: hydrogel, 3. Cell: HUVECs, 4. Cell + Gel: HUVECs mixed with hydrogel 5. Vascularized hydrogel disk) into the ischemic hind limb. Vascularized hydrogel disk significantly increased blood flow and significantly reduced tissue necrosis in the ischemic hind limb compared with the PBS-injected control group in Figure 4-7. Injection of VT significantly reduced tissue necrosis and limb loss, whereas the control group or Gel, Cell, Gel/Cell injected group exhibited severe necrosis and loss of the ischemic hind limb when inspected 4 weeks after induction of ischemia in Figure 4-8.

a

LDPI	Control	Gel	Cell	Gel / Cell	Vascularized Tissue
Day 0	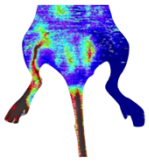	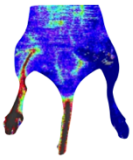	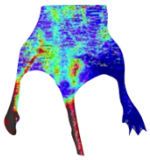	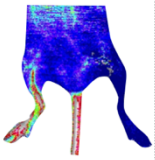	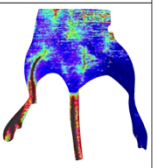
Day 28	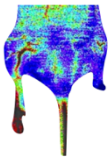	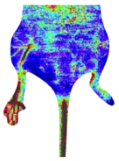	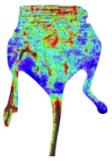	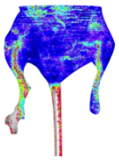	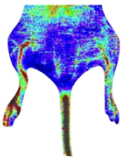
Recovery (%)	24.5 ± 5.9	36.8 ±11.0	42.1 ± 0.2	44.5 ± 9.9	60.2 ± 4.2

Figure 4-7. Effects of control released VT peptides on blood perfusion, necrosis, and neovascularization in the ischemic hind limb. Injection of VT into hind limb ischemia model resulted in enhanced blood perfusion and neovascularization. a) Representative images of a mouse hind limb injected with control, Gel, Cell, Gel/Cell, and VT on day 0 and 28.

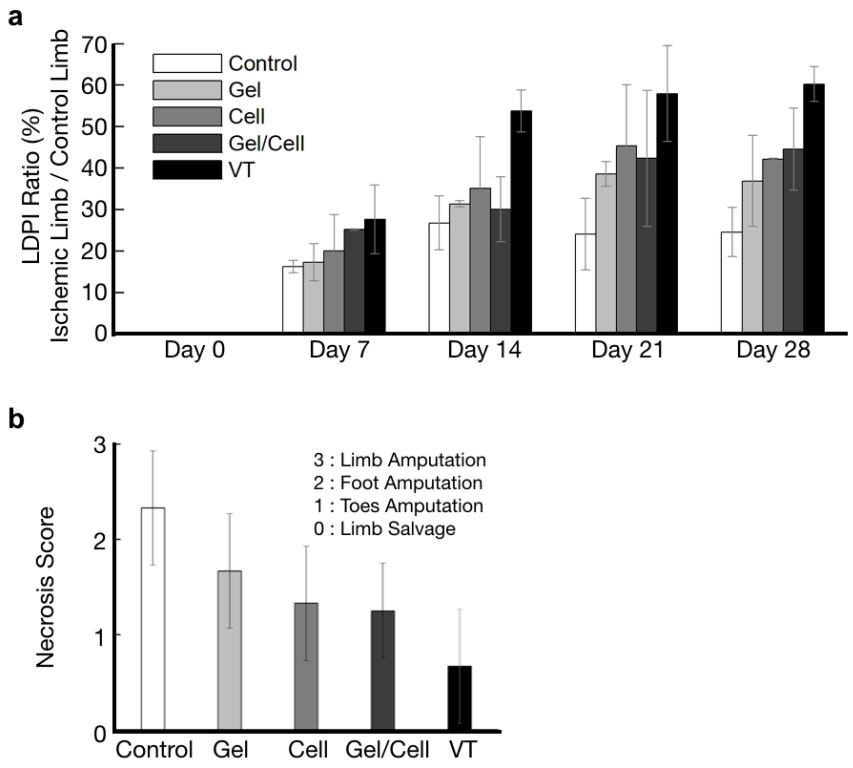

Figure 4-8. a) Quantitative analysis of blood flow measured by LDPI. The LDPI ratio was calculated as the ratio of ischemic to contralateral hind limb blood perfusion over the observation period. a) Statistical analysis of the necrosis score on day 28

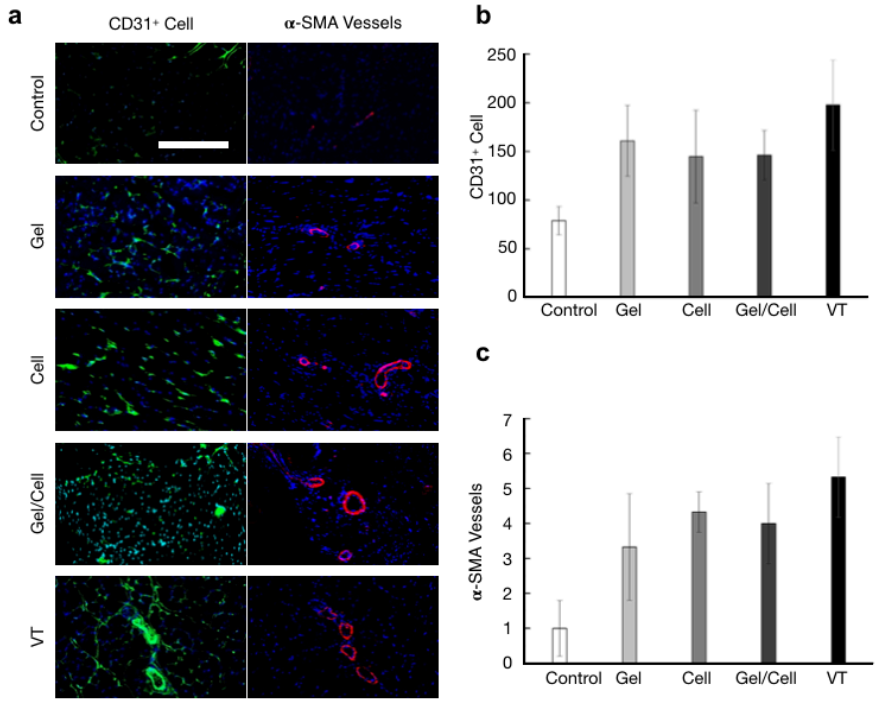

Figure 4-9. (a) Immunostaining of CD31-positive capillaries (green) or a-SMA-positive blood vessels (red) in ischemic limbs on day 28 after muscular injection. Nuclei (blue) were counterstained with DAPI and overlaid images are shown (scale bar = 30 μm). (b) Quantitative analysis of capillary density expressed by the number of CD31+ capillaries per high power field. (c) Quantitative analysis of a-SMA-positive blood vessels per high power field.

In addition, vascularized hydrogel disk significantly improved increase in CD31-positive capillaries and α-SMA-positive arteries/arterioles on day 28 after introduction of ischemia in Figure 4-9. Although the intramuscular injections of Gel only, Cell only, Cell + Gel (HUVECs mixed hydrogel) group also improved blood perfusion and angiogenesis compared with the control group, vascularized hydrogel disk showed the more significant therapeutic efficacy than these groups. These results suggest that the pre-vascularized scaffold effectively improves blood perfusion and neovascularization in the ischemic hind limb.

4-4. Conclusion

In this thesis, we have shown that transplantable vascularized tissue on a chip effectively facilitated proliferation and angiogenic activities *in vivo*. Furthermore, we have engineered 3D printed biocompatible microfluidic device for controlled vasculogenesis and transplantatio. Our animal experiments demonstrated that multiple HUVEC condition injection into hindlimb ischemia model resulted in a pro-angiogenic response. We further showed that vascularized tissue led to controlled *in vivo* release and resulted in increased therapeutic efficacy of single transplantation.

This transplantation approach has potential to address both clinical and *in vitro* needs. The ability of a vascularized tissue to completely regenerate vascular tissue voids while providing interconnected as a synthetic alternative to grafting technology. We present a fundamental change in the approach to ischemic tissue regenerative therapy by using the open microfluidic device by formation to promote the development of complex three-dimensional networks on timescales previously using current fibrinogen hydrogel technologies. Complex combinations of vascularized tissue with deterministic chemical and physical properties may enable tissue regeneration in a range of distinct physiological niches (for example, neural, cardiac, skin, and so on), where VT are tailored to

each niche via their building-block properties. The unique combination of self-detached and transplantable of VT has the potential to alter the landscape of tissue regeneration *in vivo*. The results obtained in the present study shows the angiogenic response induced by the vascularized tissue in fibrinogen hydrogel, suggesting the possibility of simplifying the vascularized tissue based therapeutic strategies.

Chapter 5

Concluding Remarks

5-1. Conclusion

In this thesis, the integrated platform of through-hole membrane and self-detached biocompatible materials on microfluidics were proposed for regenerative medicine of open microfluidic device.

In chapter 2, presents a simple approach to the fabrication of micro and nano scale through-hole membranes. The process itself is highly scalable, modular, and compatible with a very diverse range of different polymers to achieve desired specifications from hundreds of microns to hundreds of nanometers. Using this process, fabricated membranes have a high degree of uniformity of thickness, no residues, and no meniscus deformation at the through-hole sites.

In chapter 3, proposed the use of HDDA and TMPTA as biocompatible and self-detachable photopolymers as a substrate for the proposed open-access microfluidic device platform. The ability of the OAMD platform to allow for the non-destructive sampling of cultivated tissues allows for

previously impossible. The direct and nondestructive accessibility of OAMD culture systems through the use of BSP shows great promise in any research applications which require direct tissue sampling and high accessibility for structural analysis.

In chapter 4, we have shown that vascularized tissue effectively facilitated proliferation and angiogenic activities of *in vivo*. Furthermore, we have engineered biocompatible through-hole membrane for controlled separated from microfluidic device. Our animal experiments demonstrated that vascularized tissue injection into hind limb ischemia model resulted in a pro-angiogenic response. We further showed that vascularized tissue resulted in increased therapeutic efficacy of single transplantation.

This result gave a novel insight to vascularized tissue transplantation of the regenerative medicine. Regenerative medicine by the open microfluidic device may be a new promising perspective to medical treatment, such as stem cell therapy of tissue engineering.

Bibliography

[1] J. C. McDonald, D. C. Duffy, J. R. Anderson, D. T. Chiu, H. K. Wu, O. J. A. Schueller and G. M. Whitesides, "Fabrication of microfluidic systems in poly(dimethylsiloxane)", Electrophoresis, 2000, 21, 27-40.

[2] K. Ziolkowska, R. Kwapiszewski and Z. Brzozka," Microfluidic devices as tools for mimicking the in vivo environment", New J. Chem., 2011, 35, 979-990.

[3] A. R. Wheeler, W. R. Throndset, R. J. Whelan, A. M. Leach, R. N. Zare, Y. H. Liao, K. Farrell, I. D. Manger and A. Daridon, "Microfluidic Device for Single-Cell Analysis", Anal. Chem., 2003, 75, 3581-3586.

[4] P. S. Dittrich and A. Manz, "Lab-on-a-chip: microfluidics in drug discovery", Nat Rev Drug Discov, 2006, 5, 210-218.

[5] S. N. Bhatia and D. E. Ingber, "Microfluidic organs-on-chips", Nat Biotechnol, 2014, 32, 760-772.

[6] D. Huh, H. J. Kim, J. P. Fraser, D. E. Shea, M. Khan, A. Bahinski, G. A. Hamilton and D. E. Ingber, "Microfabrication of human organs-on-chips", Nat. Protoc., 8, 11, 2013, 2135.

[7] D. Huh, B. D. Matthews, A. Mammoto, M. Montoya-Zavala, H. Y. Hsin and D. E. Ingber, "Reconstituting organ-level lung functions on a chip", Science, 2010, 328, 1662-1668.

[8] H. J. Kim, D. Huh, G. Hamilton and D. E. Ingber, “Human gut-on-a-chip inhabited by microbial flora that experiences intestinal peristalsis-like motions and flow”, Lab Chip, 2012, 12,2165-2174.

[9] K. J. Jang, A. P. Mehr, G. A. Hamilton, L. A. McPartlin, S. Y. Chung, K. Y. Suh and D. E. Ingber, “Human kidney proximal tubule-on-a-chip for drug transport and nephrotoxicity assessment”, Integr. Biol., 2013, 5, 1119-1129.

[10] D. C. Duffy, J. C. McDonald, O. J. A. Schueller and G. M. Whitesides, “Rapid Prototyping of Microfluidic Systems in Poly(dimethylsiloxane)”, Anal. Chem., 1998, 70, 4974-4984.

[11] E. Ostuni, R. Kane, C. S. Chen, D. E. Ingber and G. M. Whitesides, “Patterning Mammalian Cells Using Elastomeric Membranes”, Langmuir, 2000, 16, 7811-7819.

[12] H. Chen, J. Sun, E. Wolvetang and J. Cooper-White, “High-throughput, deterministic single cell trapping and long-term clonal cell culture in microfluidic devices”, Lab Chip, 2015, 15, 1072-1083.

[13] A. Folch, B. H. Jo, O. Hurtado, D. J. Beebe and M. Toner, “Microfabricated elastomeric stencils for micropatterning cell cultures”, J. Biomed. Mater. Res., 2000, 52, 346-353.

[14] T. S. Santisteban, R. Zengerle and M. Meier, “Through-holes, cavities and perforations in polydimethylsiloxane (PDMS) chips”, RSC Adv., 2014, 4, 48012-48016.

[15] S. Y. Chou, P. R. Krauss and P. J. Renstrom, “Nanoimprint lithography”, J. Vac. Sci. Techol., 1996, 14, 4129-4133.

[16] E. Kim, Y. Xia and G. M. Whitesides, “Micromolding in Capillaries: Applications in Materials Science”, J. Am. Chem. Soc., 1996, 118, 5722-5731.

[17] Y. Xia, E. Kim and G. M. Whitesides, “Micromolding of Polymers in Capillaries: Applications in Microfabrication”, Chem. Mater., 1996, 8, 1558-1567.

[18] E. Kim, Y. Xia and G. M. Whitesides, “Two- and three-dimensional crystallization of polymeric microspheres by micromolding in capillaries”, Adv. Mater., 1996, 8, 245-247.

[19] N. L. Jeon, I. S. Choi, B. Xu and G. M. Whitesides, “Large-Area Patterning by Vacuum-Assisted Micromolding”, Adv. Mater., 1999, 11, 946-950.

[20] R. Wei, D. Pedone, A. Zurner, M. Doblinger and U. Rant, “Fabrication of Metallized Nanopores in Silicon Nitride Membranes for Single-Molecule Sensing”, Small, 2010, 6, 1406-1414.

[21] H. Cho, J. Kim, H. Park, J. Won Bang, M. Seop Hyun, Y. Bae, L. Ha, D. Yoon Kim, S. Min Kang, T. Jung Park, S. Seo, M. Choi and K. Y. Suh, "Replication of flexible polymer membranes with geometry-controllable nano-apertures via a hierarchical mould-based dewetting", Nat Commun, 2014, 5, 3137.

[22] R. Vendamme, S. Y. Onoue, A. Nakao and T. Kunitake, "Robust free-standing nanomembranes of organic/inorganic interpenetrating networks", Nat. Mater., 2006, 5, 494-501.

[23] C. C. Harrell, Z. S. Siwy and C. R. Martin, "Conical nanopore membranes: controlling the nanopore shape" Small, 2006, 2, 194-198.

[24] C. A. Baker, L. K. Bright and C. A. Aspinwall, "Photolithographic fabrication of microapertures with well-defined, three-dimensional geometries for suspended lipid membrane studies", Anal. Chem., 2013, 85, 9078-9086.

[25] A. J. Bennett, D. L. Ringach, "Animal Research in Neuroscience: A Duty to Engage", Neuron. 2016, 92, 2, 653–657

[26] C. P. Huang, J. Lu, H. Seon, A. P. Lee, L. A. Flanagan, H. Kim, A. J. Putnam and N. L. Jeon, "Engineering microscale cellular niches for three-dimensional multicellular co-cultures", Lab Chip. 2009, 9, 1740–1748

[27] S. J. Trietsch, E. Naumovska, D. Kurek, M. C. Setyawati, M. K. Vormann, K. J. Wilschut, H. L. Lanz, A. Nicolas, C. P. Ng, J. Joore, S. Kustermann, A. Roth, T. Hankemeier, A. Moisan and P. Vulto, "Membrane-free culture and real-time barrier integrity assessment of perfused intestinal epithelium tubes", Nat. Comm., 2017, 8, 262

[28] S. Kim, H. Lee, M. Chung, N. L. Jeon, "Engineering of functional, perfusable 3D microvascular networks on a chip", Lab Chip. 2013, 13(8), 1489–1500

[29] P. J. Lee, P. J. Hung and L. P. Lee, "An artificial liver sinusoid with a microfluidic endothelial-like barrier for primary hepatocyte culture", Biotechnol. Bioeng., 2007, 97(51), 1340–1346

[30] E. W. Esch, A. Bahinski and D. Huh, "Organs-on-chips at the frontiers of drug discovery", Nat. Rev. Drug. Discov., 2015, 14, 248-260

[31] S. N. Bhatia, D. E. Ingber, "Microfluidics: The Challenge Is to Bridge the Gap Instead of Looking for a 'Killer App'", Nat. Biotechnol. 2014, 32, 760–776

[32] K. J. Jang, M. S. Kim, D. Feltrin, N. L. Jeon, K. Y. Suh, O. Pertz, "Two Distinct Filopodia Populations at the Growth Cone Allow to Sense Nanotopographical Extracellular Matrix Cues to Guide Neurite Outgrowth", PLoS One 2010, 5, e15966

[33] S. G. Lipson, H. Lipson, D. S. Tannhauser, Optical Physics, book,

[34] J. Havrankova, J. Roth, M. Brownstein, “Insulin receptors are widely distributed in the central nervous system of the rat”, Nature. 1978, 272, 827–829

[35] P. M. Richardson, U. M. McGuinness, A. J. Aguayo. “Axons from CNS neurones regenerate into PNS grafts”,Nature. 1980, 284, 264–265

[36] B. A. Brody, H. C. Kinney, A. S. Kloman, F. H. Gilles, “Sequence of central nervous system myelination in human infancy. I. An autopsy study of myelination”, J Neuropathol Exp Neurol 1987, 46, (3), 283–301

[37] G. A. Wright, L. Costa, A. Terekhov, D. Jowhar, W. Hofmeister, C. Janetopoulos, “On-Chip Open Microfluidic Devices for Chemotaxis Studies”, Microsc. Microanal. 2012, 18, 816–828

[38] X. Li, Y. Tao, D. H. Lee, H. K. Wickramasinghe, A. P. Lee, “In situ mRNA isolation from a microfluidic single-cell array using an external AFM nanoprobe”, Lab Chip, 2017, 17, 9, 1635–1644

[39] S. Lone, J. M. Zhang, I. U. Vakarelski, E. Q. Lim, S. T. Thoroddsen, “Evaporative Lithography in Open Microfluidic Channel Networks”, Langmuir. 2017, 33, 2861−2871

[40] Ouriel K. Peripheral arterial disease. "Peripheral arterial disease", Lancet 2001;358:1257-64.

[41] Selvin E, Erlinger TP. "Prevalence of and risk factors for peripheral arterial disease in the United States - Results from the National Health and Nutrition Examination Survey", 1999-2000. Circulation 2004, 110:738-43.

[42] Luther M, Lepantalo M, Alback A, Matzke S. "Amputation rates as a measure of vascular surgical results", Brit J Surg 1996;83:241-4.

[43] Bryant DM, Mostov KE (2008) “From cells to organs: Building polarized tissue. Nat Rev Mol Cell Biol 9(11):887–901.

[44] Lutolf MP, Hubbell JA “Synthetic biomaterials as instructive extracellular microenvironments for morphogenesis in tissue engineering”, Nat Biotechnol 2005, 23(1): 47–55.

[45] Stevens MM, George JH “Exploring and engineering the cell surface interface”, Science 2005, 310(5751):1135–1138.

[46] Langer R, Tirrell DA “Designing materials for biology and medicine”, Nature 2014, 428(6982):487–492.

[47] Khademhosseini A, Langer R, Borenstein J, Vacanti JP “Microscale technologies for tissue engineering and biology”, Proc Natl Acad Sci USA 2006, 103(8):2480–2487.

[48] Steinke M, et al. “An engineered 3D human airway mucosa model based on an SIS scaffold”, Biomaterials, 2014, 35(26):7355–7362.

[49] Wang J, et al. “Phage nanofibers induce vascularized osteogenesis in 3D printed bone scaffolds”, Adv Mater, 2014, 26(29):4961–4966.

[50] Jakab K, Neagu A, Mironov V, Markwald RR, Forgacs G, “Engineering biological structures of prescribed shape using self-assembling multicellular systems”, Proc Natl Acad Sci USA 2014, 101(9):2864–2869.

[51] Jang JH, Castano O, Kim HW, “Electrospun materials as potential platforms for bone tissue engineering”, Adv Drug Deliv Rev, 2009, 61(12):1065–1083.

[52] Gross BC, Erkal JL, Lockwood SY, Chen C, Spence DM, “Evaluation of 3D printing and its potential impact on biotechnology and the chemical sciences”, Anal Chem 2014, 86(7):3240–3253.

[53] Murphy SV, Atala A, “3D bioprinting of tissues and organs”, Nat Biotechnol, 2014, 32(8): 773–785.

[54] Schubert C, van Langeveld MC, Donoso LA, “Innovations in 3D printing: A 3D overview from optics to organs”, Br J Ophthalmol, 2014, 98(2):159–161.

[55] J. Zhang, K. L. Tan, G. D. Hong, L. J. Yang and H. Q. Gong, "Polymerization optimization of SU-8 photoresist and its applications in microfluidic systems and MEMS", J. Micromech. Microeng., 2001, 11, 20-26.

[56] S. N. Jae Woo Park, Myeongwoo Kang, Sang Jun Sim, Noo Li Jeon, "PDMS microchannel surface modification with Teflon for algal lipid research", BioChip J, 2017, DOI: 10.1007/s13206-017-1302-0, 8.

[57] S. J. Choi, P. J. Yoo, S. J. Baek, T. W. Kim and H. H. Lee, "An Ultraviolet-Curable Mold for Sub-100-nm Lithography", J. Am. Chem. Soc., 2004, 126, 7744-7745.

[58] J. Park, D. Tahk, C. Ahn, S. G. Im, S. Choi, K. Suh and S. Jeon, "Conformal phase masks made of polyurethane acrylate with optimized elastic modulus for 3D nanopatterning", J. Mater. Chem. C, 2014, 2, 2316.

[59]. M. Laroussi, "Low temperature plasma-based sterilization: overview and state-of-the-art", Plasma Process. Polym. **2005**, 2, 391–400

[60] D. Tahk, T. I. Kim, H. Yoon, M. Choi, K. Shin, K. Y. Suh, "Fabrication of antireflection and antifogging polymer sheet by partial photopolymerization and dry etching", Langmuir 2010, 26 (4), 2240–2243

[61] G. Bartzokis, P. H. Lu, J.Mintz, “Human brain myelination and amyloid beta deposition in Alzheimer's disease
”, Alzheimers Dement 2007, 3, 122–125.

[62] N. Baumann, D. Pham-Dinh, “Biology of oligodendrocyte and myelin in the mammalian central nervous system”, Physiol. Rev. 2001, 81, 871–927.

[63] K. R. Jessen, R. Mirsky, “Negative regulation of myelination: relevance for development, injury, and demyelinating disease”, Glia 2008, 56, 1552–1565.

[64] U. Suter, S. S. Scherer, “Disease mechanisms in inherited neuropathies”, Nat Rev Neurosci 2003, 4, 714–726.

[65] S. Hyung, B. Yoon Lee, J. C. Park, J. Kim, E. M. Hur, J. K. Francis Suh, “Coculture of Primary Motor Neurons and Schwann Cells as a Model for In VitroMyelination”, Sci Rep. 2015, 5, 15122

[66] H. Honkanen, O. Lahti, M. Nissinen, R. M. Myllylä, S. Kangas, S. Päiväläinen, M. H. Alanne, S. Peltonen, J. Peltonen, A. M. Heape, “Isolation, purification and expansion of myelination-competent, neonatal mouse Schwann cells”, Eur J Neurosci, 2007, 26, 953–964.

[67] S. Päiväläinen, M. Nissinen, H. Honkanen, O. Lahti, S. M. Kangas, J. Peltonen, S. Peltonen and A. M. Heape, “Myelination in mouse dorsal

root ganglion/Schwann cell cocultures", Mol Cell Neurosci, 2008, 37, 568–578.

[68] A. M. Taylor, M. Blurton-Jones, S. W. Rhee, D. H. Cribbs, C. W. Cotman, N. L. Jeon. "A microfluidic culture platform for CNS axonal injury, regeneration and transport", Nat Methods, 2005, 2, 599–605.

[69] M. Gingras, M. M. Beaulieu, V. Gagnon, H. D. Durham, F. Berthod, "In vitro study of axonal migration and myelination of motor neurons in a three-dimensional tissue-engineered model", Glia, 2008, 56, 354–364.

[70] K. Haastert, J. Grosskreutz, M. Jaeckel, C. Laderer, J. Bufler, C. Grothe, P. Claus. "Rat embryonic motoneurons in long-term co-culture with Schwann cells—a system to investigate motoneuron diseases on a cellular level in vitro", J Neurosci Methods, 2005, 142, 275–284.

[71] J. A. Pereira, F. Lebrun-Julien, U. Suter, "Molecular mechanisms regulating myelination in the peripheral nervous system", Trends Neurosci, 2012, 35, 123–134.

[72]. S. Bang, S. Na, J. M. Jang, J. Kim, N. L. Jeon, "Engineering-Aligned 3D Neural Circuit in Microfluidic Device", Adv Healthc Mater. **2016**, 5(1), 159–166

[73] U. W. Gedde, Polymer Physics, Book.

[74] Y. –C. Lai, L. J. Baccei, “Synthesis and structure–property relationships of UV-curable urethane prepolymers with hard–soft–hard blocks”, J Appl Polym Sci 1991, 42, 7, 2039–2044.

[75] A. Banerjee, M. Arha, S. Choudhary, R. S. Ashton, S. R. Bhatia, D. V. Schaffer, and R. S. Kane, “The influence of hydrogel modulus on the proliferation and differentiation of encapsulated neural stem cells.”, Biomaterials, 2009, 30 (27), 4695–4699.

[76] M. P. Sousa, S. G. Caridade, and J. F. Mano, “You have full text access to this content

Cell Alignment: Control of Cell Alignment and Morphology by Redesigning ECM-Mimetic Nanotopography on Multilayer Membranes”, Adv Healthc Mater, 2017, 6, 15, 9

[77] A. M. Ross, Z. Jiang, M. Bastmeyer, J. Lahann, “Physical aspects of cell culture substrates: topography, roughness, and elasticity”, Small 2012, 8, 3, 336–355.

[78] J. P. Mazzoccoli, D. L. Feke, H. Baskaran, and P. N. Pintauro, “Mechanical and cell viability properties of crosslinked low-and high-molecular weight poly (ethylene glycol) diacrylate blends”, J. Biomed. Mater. Res. Part A, 2010, 93, 2, 558–566.

[79] G. Charras, E. Sahai, “Physical influences of the extracellular environment on cell migration”, Nat Rev Mol Cell Biol 2014, 15, 813–824.

[80] J. Y. Rho, R. B. Ashman, C. H. Turner, “Young's modulus of trabecular and cortical bone material: Ultrasonic and microtensile measurements”, J. Biomech 1993, 26, 2, 111-119.

국 문 초 록

말초 동맥 질환의 치료제를 개발하기 위하여 다공성 맴브레인을 지닌 개방형 마이크로 유체 장치를 개발하여 새로운 개방형 장기모사 칩을 활용한 혈관 배양 및 이식 시스템의 재생 의학적 치료제로서의 접근 가능성을 연구하였다. 말초 동맥 질환의 경우 일반적으로 동맥 또는 소동맥의 하부에서 혈관이 막혀 혈액 공급이 원활하지 못하여 조직이 괴사하게 되는 질환을 말하는데 말기 상태, 즉 조직이 괴사하기 전까지 큰 자각증상이 없는 것이 특징이다. 이러한 말초 동맥질환의 치료를 위해서는 초기에는 약물 치료를 진행하고 말기에는 조직 이식을 통하여 혈류를 회복 시키고 궁극적으로 말초 동맥 질환을 치료한다. 본 연구는 말초동맥질환의 말기 상태의 병변을 치료하기 위해 관류가 이루어진 상태의 조직을

미세유체칩에서 먼저 배양 후 괴사 조직에 이식하여 우회 혈관을 생성하고 궁극적으로 말초 동맥 질환을 치료하기 위한 장기모사칩용 개방형 미세유체칩을 설계하고 증명하였다. 이식용 미체유체칩을 개발하기 위하여 먼저 혈관 조직을 잘 배양하고 이식 가능한 환경으로 조직의 손상 없이 미세유체칩을 개방하여야 한다. 따라서 선 조건이 혈관 조직의 배양을 위하여 6 well plate 에 기반한 큰 조직의 배양과 원활한 배지 공급을 위하여 대면적 다공성 맴브레인을 제조하는 신공정 기술을 개발하였다. 그리고 개방형 미세 유체칩 환경을 구사하기 위하여 기존에 잘 알려진 생체적합성 광경화 고분자인 PEG-DA 라는 물질과 전자재료 분야에서 값싸게 많이 사용되었으나 바이오 공학 분야에는 잘 알려지지 않은 TMPTA, HDDA 광경화성 물질을 도입하여 광경화에 따른 다공성

맴브레인 제조 공정의 장점을 극대화 하였다. 재료 자체에 내재되어있는 흡습성을 이용하여 혈관 형성 초기에는 닫힌 상태의 미세유체칩의 형상으로 자가 정렬된 혈관 조직을 잘 형성하고 배양과 동시에 맴브레인이 분리되는 시스템을 구축하였다. 이를 이용하여 얻어진 혈관조직을 말초 동맥질환의 동물모델인 하지 허혈 동물 모델에 이식하여 비교군과 비교하였을 때 재혈류량이 가장 높게 증가하는 것을 확인 하였다. 본 연구에서 개발한 개방형 마이크로 유체 장치에서 배양된 혈관조직의 재생의학적 접근은 그동안 시도 되지 않는 새로운 시각의 접근이라 할 수 있다. 이를 통해 말초 동맥 질환의 치료 뿐만 아니라 다양한 질병의 치료에 있어서 조직 공학 분야에서의 새로운 접근 방식을 제시하고자 한다.

주요어: 미세유체칩, 맴브레인, 생체적합성, 자외선경화, 조직공학

학번: 2010-30797